c\

A STUDY OF ISOTROPIC STRUCTURE IN ATMOSPHERIC BOUNDARY LAYER TURBULENCE

by

IAN TAYLOR WEBSTER

B.Sc., University of British Columbia

A THESIS SUBMITTED IN PARTIAL FULFILMENT OF THE

REQUIREMENTS FOR THE DEGREE OF

MASTER OF SCIENCE

in the Department

of

Physics

and the Institute of Oceanography

We accept this thesis as conforming to the

required standard

THE UNIVERSITY OF BRITISH COLUMBIA

June 1972

ABSTRACT

The two purposes of this study were to determine at what turbulent scales in a high Reynold's number shear flow the transition to isotropy occurs and at what scales Taylor's 'frozen field' hypothesis is applicable. The flow studied was the wind at a height of $z = 2$ m. above a flat land surface. Four hot wire anemometers were mounted in a three dimensional array to collect data on the downwind turbulent velocity fluctuations. Cross spectra were computed from the observed data between three pairs of hot wires having the same spacing in different directions; these were varied between 1.8 m. and 2 cm. Knowing the observed spectrum of downwind velocity fluctuations and assuming the turbulence is isotropic, incompressible and obeys Taylor's hypothesis, theoretical cross spectra were computed. The results of the comparison between the observed and theoretical cross spectra for different spacings revealed that in the flow studied the behaviour of the turbulence is consistent with the assumptions of both isotropy and Taylor's hypothesis for $k_1z > 20$, but for wave numbers less than this range either or both of the assumptions are not valid. However, between $k_1z = 4$ and $k_1z = 20$ the turbulence appears to be at least axisymmetric about the downstream direction and for $k_1z > 3$ that part of Taylor's hypothesis relating observed frequency at a stationary sensor to the downstream wave number component appears to be justified.

TABLE OF CONTENTS

LIST OF TABLES

LIST OF FIGURES

ACKNOWLEDGEMENTS

I wish to thank the many staff and students of the Institute of Oceanography, University of British Columbia who have assisted me in this project either with their advice or with their physical labour. I am indebted to Dr. R.W. Burling, my research supervisor, for his many suggestions especially in connection with the preparation of this thesis and to Drs. G.S. Pond and R.W. Stewart for much essential advice.

Thanks are due also to Captain D.W. Bastock, Commanding Officer of the Canadian Forces Station at Ladner, for kindly making the site available for the experiment.

Finally, I am grateful to the Department of Mechanical Engineering at U.B.C. for permitting me to use their wind tunnel facilities and for determining the vibrational characteristics of the probe supports.

This work was done in conjunction with the Air-Sea Interaction Programme of the Institute of Oceanography and was supported by the Defence Research Board and by the National Research Council of Canada.

Chapter 1

INTRODUCTION

To date the Navier Stokes equations have not been solved for high Reynold's number shear flow. For high enough Reynold's numbers it has been postulated that there exists a subrange of isotropic turbulence scales in which no production and no dissipation of energy take place and in which energy is transferred from scale to smaller scale by inertial processes only. In this 'inertial subrange' Kolmogoroff (1941) predicted behaviour for structure functions which is equivalent to the one dimensional power spectra of turbulent velocity fluctuations being proportional to '$k_1^{-5/3}$' where k_1 is the downstream wave number. A wave number range in which the spectra have the '-5/3' form has been observed on numerous occasions; for example in atmospheric boundary layer flow by Pond *et al* (1963) and in oceanic turbulence by Grant, Stewart and Moilliet (1962). The '$k_1^{-5/3}$' spectra of downstream velocity fluctuations observed by Pond *et al* (1963) and many others extend to wave numbers low enough that the turbulence is clearly anisotropic.

In a shear flow energy is transferred into the turbulence because of the interaction between the turbulent stresses and the mean velocity shear. Since this process causes energy transfer directly into the velocity component along the mean flow, the turbulence, at the scales involved in the transfer, is necessarily anisotropic; that is it is not symmetrical in all spatial directions. This energy is passed to smaller scales by non-linear velocity interactions and at the same time is redistributed by action of the pressure among the three velocity components. One might expect that as the energy passes down the scales memory of the anisotropic sources at large scales will tend to disappear and that eventually the turbulence will appear to be essentially isotropic at sufficiently small scales. Pond *et al* (1963) estimated a lower wave number limit for isotropy in a turbulent shear flow at distance z from a boundary as $k_1 z > 4.5$. This result was based on the determination of the scale of turbulence at which the rate of strain due to the turbulence itself becomes as big as the rate of strain due to the mean shear in a flow which conforms to the logarithmic law of the wall and in which the local dissipation of turbulent energy equals the local production.

A number of experimental attempts have been made to determine at what scales a turbulent shear flow does become isotropic. Using hot wire anemometers (in x-configuration at a single point) Weiler (1966) estimated the ratio of the vertical velocity spectrum to the downwind velocity spectrum and the turbulent shear stress in the boundary layer a few meters above the sea. In an isotropic inertial subrange the ratio of the velocity spectra is predicted to be 4/3, but the ratio observed was less than 1.1 (except on a few occasions) at scales only slightly larger than the dissipation scales. Also, in an inertial subrange the turbulent shear stress must be zero. Although the observed shear stresses were non zero for wave numbers above Pond's limit of isotropic wave numbers the degree of anisotropy associated with this property appeared to be fairly small. Van Atta and Chen (1970) determined a lower wave number limit for isotropy in the atmospheric boundary layer over the sea. Their lower limit, $k_1 z = \pi$, was based on the comparison of observed second order structure functions with those predicted for the inertial subrange.

The primary objective of my study was to determine by another means at what scales the transition to isotropy might occur in a high Reynold's number shear flow. The measurements were made in a wind at a height of 2 m. over a flat land surface. This type of flow is sometimes close to the simplest form of shear flow in which a steady mean wind is parallel to the ground, does not change direction with height and which possesses negligible local heat sources of energy. For the sections of data analyzed the durations of observations of the wind are much shorter than the time scales associated with changing synoptic atmospheric conditions.

The degree of isotropy in the turbulence was studied by comparing cross spectra between downwind components at separated points with those expected theoretically. The turbulence data were obtained from a three dimensional array of four hot wire anemometers. If the turbulence is in an incompressible fluid, is assumed to be isotropic and if also Taylor's 'frozen field' hypothesis holds it is possible to compute theoretical cross spectra from the observed power spectra of downwind velocity fluctuations.

A stationary velocity sensor senses some property related to the velocity fluctuations at a given point in space as a function of time. Observed cross spectra are obtained as functions of frequency but the theoretical cross spectra are derived in terms of wave numbers. However, the observed cross spectra can be transformed into a wave number space by assuming that the turbulence is transported in accordance with Taylor's hypothesis, which is that the turbulence transports like a 'frozen field' and does not change its structure or its advection velocity while advecting through distances comparable with the scales of turbulence studied. Under this hypothesis, observed frequencies, f, are equivalent to downstream wave numbers, k_1, where $k_1 = \frac{2\pi f}{U}$. Since Taylor's hypothesis plays such an integral part in the comparison between the observed and theoretical cross spectra the results of the comparison depend strongly on the validity of this hypothesis. To obtain information on the validity of Taylor's hypothesis was a secondary objective of my study.

Attempts have been made by various authors to determine theoretically the conditions under which Taylor's hypothesis can be applied in a turbulent shear flow. Lin (1953) theorized that the effect of distortion of eddies by the mean shear would be small provided the advection of strain rate in the downstream direction is very much larger than the turbulent advection of strain rate across the shear. This criterion, applied to the condition of the flow during my measurements and assuming a logarithmic mean velocity profile requires that $k_1 z \gg 0.2$. Lin also describes conditions under which the rate of distortion in the turbulence due to pressure fluctuations can be considered to be negligible. The criterion he obtains for applicability of Taylor's hypothesis in this case is $5\overline{u_1^2}/U^2 \ll 1$. Typical values of $5\overline{u_1^2}/U^2$ encountered in the present study were about 0.15.

A third assumption involved in the derivation of theoretical cross spectra is that the turbulence behaves as if it were incompressible. Hinze (1959) estimates the compressibility effect to be negligible if $\overline{u^2}/c^2 \ll 1$ where u is the magnitude of the velocity fluctuations and c is the speed of sound under the measuring conditions. For the present study the above ratio was of order 10^{-5} making incompressibility a good assumption. Because incompressibility is such a good approximation the results of the comparison of observed and theoretical cross spectra should depend primarily on the validity of the two assumptions; isotropy and Taylor's hypothesis.

Chapter 2

BACKGROUND

Spectral Description

In order to describe the turbulence a cartesian coordinate system $\underset{\sim}{r} = (x, y, z)$ is chosen such that the 'x' axis is in the horizontal direction directed up the mean wind, $\underset{\sim}{U}$, 'z' is the axis perpendicularly upwards, and the 'y' axis is horizontal and transverse to the mean wind. It is desirable to decompose the velocity field into the fluctuating part, $\underset{\sim}{u} = (u, v, w)$, and the mean wind, $\underset{\sim}{U} = (U, 0, 0)$. The two quantities, $\underset{\sim}{U}$ and $\underset{\sim}{u}$, are defined such that the time averages $\overline{\underset{\sim}{U}} = \underset{\sim}{U}$ and $\overline{\underset{\sim}{u}} = 0$.

Consider the product of the velocity components u_i and u_j measured at the two positions in space, $\underset{\sim}{r}$ and $\underset{\sim}{r} + \underset{\sim}{\delta}$, respectively. Provided u_i and u_j are stationary and homogeneous in the statistical sense, we can define a Fourier representation of the product of the velocities averaged over all space and all time for the n^{th} realization of the flow as: (for example, see Lumley and Panofsky, 1964, p. 25).

$$\overline{u_i^{(n)}(\underset{\sim}{r},t)\, u_j^{(n)}(\underset{\sim}{r}+\underset{\sim}{\delta},t)}^{\underset{\sim}{r},t} = \int_{-\infty}^{\infty} \Phi_{ij}^{(n)}(\underset{\sim}{k})\, e^{i\underset{\sim}{k}\cdot\underset{\sim}{\delta}}\, d\underset{\sim}{k} \tag{2.1}$$

where $d\underset{\sim}{k}$ is an element of volume in $\underset{\sim}{k} = (k_1, k_2, k_3)$ space and $\Phi_{ij}^{(n)}$ is the spectral density tensor for the n^{th} realization.

We can introduce a cross spectral tensor, $Cr_{ij}^{(n)}(\underset{\sim}{k}, \underset{\sim}{\delta})$, defined precisely in Appendix A, which has the property that:

$$\overline{u_i^{(n)}(\underset{\sim}{r},t)u_j^{(n)}(\underset{\sim}{r}+\underset{\sim}{\delta},t)}^{\underset{\sim}{r},t} = \int_{-\infty}^{\infty} Cr_{ij}^{(n)}(\underset{\sim}{k},\underset{\sim}{\delta})\, d\underset{\sim}{k} \tag{2.2}$$

Thus $Cr_{ij}^{(n)}(\underset{\sim}{k},\underset{\sim}{\delta})$ is the contribution to the total covariance $\overline{u_i^{(n)}(\underset{\sim}{r},t)u_j^{(n)}(\underset{\sim}{r}+\underset{\sim}{\delta},t)}^{\underset{\sim}{r},t}$

per unit wave number volume at $\underset{\sim}{k}$.

The smoothed cross spectrum, $Cr_{ij}(\underset{\sim}{k},\underset{\sim}{\delta})$, is the ensemble average of the $Cr_{ij}^{(n)}(\underset{\sim}{k},\underset{\sim}{\delta})$ over an infinite number of realizations of the flow (Lumley and Panofsky, 1964).

$$Cr_{ij}(\underset{\sim}{k},\underset{\sim}{\delta}) = \left\langle Cr_{ij}^{(n)}(\underset{\sim}{k},\underset{\sim}{\delta}) \right\rangle_{n=1,\infty} \qquad (2.3)$$

The theoretical cross spectra, $Cr_{ij}^{T}(\underset{\sim}{k},\underset{\sim}{\delta})$, are defined to be averaged in the manner of (2.3). (The terminology Cr^{T} denotes a theoretical cross spectrum and Cr^{O} an observed cross spectrum.)

In the experiment just the one dimensional observed cross spectra, $Cr_{ij}^{O}(k_1,\underset{\sim}{\delta})$, can be obtained. Furthermore, the $Cr_{ij}^{O}(k_1,\underset{\sim}{\delta})$ are only estimates of the ideal, smoothed, one dimensional cross spectra because the average, $\overline{u_i(\underset{\sim}{r},t)u_j(\underset{\sim}{r}+\underset{\sim}{\delta},t)}^{\underset{\sim}{r},t}$, ideally over all space and all time, can only be approximated as an average over finite time and because the ensemble average can only be over a finite number of realizations of the flow. The theoretical and the observed one dimensional cross spectra are estimated in Appendices A and B respectively.

When $\underset{\sim}{\delta} = 0$ and $i = j$ the $Cr_{ij}(k_1,\underset{\sim}{\delta})$ are the one dimensional power spectra, $\Phi_i(k_1)$.

$$\Phi_i(k_1) = Cr_{ii}(k_1,0) \quad \text{(not summed over i)} \qquad (2.4)$$

The physical interpretation of $\Phi_u(k_1)$, the one dimensional power spectrum of downstream velocity fluctuations, is that it is the contribution to the total variance $\overline{u^2}$, per unit wave number, k_1, from all wave numbers, $\underset{\sim}{k}$, having the component, k_1.

In this study the cospectrum, $Co(k_1,\delta)$, and the quadspectrum, $Qu(k_1,\delta)$ are defined as the real and imaginary parts of $Cr_{11}(k_1,\underset{\sim}{\delta})$ which is the one dimensional cross spectrum of downstream velocity fluctuations.

Thus:

$$Co(k_1,\underset{\sim}{\delta}) = Re\left(Cr_{11}(k_1,\underset{\sim}{\delta})\right) \tag{2.5}$$

$$Qu(k_1,\underset{\sim}{\delta}) = Im\left(Cr_{11}(k_1,\underset{\sim}{\delta})\right) \tag{2.6}$$

The cospectrum is a measure of the amount of 'in phase' coherent energy density as a function of k_1 between the velocities at $\underset{\sim}{r}$ and $\underset{\sim}{r}+\underset{\sim}{\delta}$, whereas the quadspectrum is a measure of the coherent energy density which is 90° out of phase at the same two points.

$\Phi_u(k_1)$, $Co(k_1,\underset{\sim}{\delta})$ and $Qu(k_1,\delta)$ together define the coherence, $Coh(k_1,\delta)$, which is a measure of the normalized coherent energy density between the points, $\underset{\sim}{r}$ and $\underset{\sim}{r}+\underset{\sim}{\delta}$.

$$Coh(k_1,\underset{\sim}{\delta}) = \frac{\left[\left(Co(k_1,\underset{\sim}{\delta})\right)^2+\left(Qu(k_1,\underset{\sim}{\delta})\right)^2\right]^{\frac{1}{2}}}{\Phi_u(k_1)} \tag{2.7}$$

The relative phase, α, of the coherent energy density between the points, $\underset{\sim}{r}$ and $\underset{\sim}{r} + \underset{\sim}{\delta}$ is given by:

$$\alpha = \tan^{-1}\left(\frac{Qu(k_1,\underset{\sim}{\delta})}{Co(k_1,\underset{\sim}{\delta})}\right) \tag{2.8}$$

The Experimental Arrangement

The isotropy of the turbulence was studied by estimating the cross spectra between velocity components observed simultaneously using hot wire anemometers at four points with selected space separations. The ideal set of separations would be to have one sensor situated at an 'origin' of the coordinate system (x, y, z) and the others each at equal distance along the three coordinate axes. The arrays used were designed so the upwind arm was offset in the horizontal plane to avoid wake interference to the sensor at the origin. In practice the coordinate system was always determined by the direction of the mean wind as illustrated in Figure 1 which shows the physical arrangement of the sensor systems. The angle, θ, was some angle between 10° and 20° during each data run.

The concept of 'scale' in turbulence suggests the optimum information on the isotropy at some scale can be obtained by examining cross spectra at separations up to about the scale distance. The height of the three sensors in the horizontal plane was 2 m., so using the criterion (Pond et al, 1963), the lower limit of wave numbers expected to be isotropic is somewhat above $k_1 \approx 4.5(2m)^{-1} \approx 2.2m^{-1}$. If turbulent scale size be taken as $\frac{2\pi}{k_1}$ then isotropy is not expected at scales greater than 2m. or so. The largest separation, 1.8 m., used in the measurements was chosen as representative of the possible upper limit of scales in the inertial subrange. The closest separation of the sensors was 2 cm. which was the smallest practically measurable spacing under the conditions of the experiment. This separation describes the smallest scales which might be expected to be within the inertial subrange near the dissipation end of the spectrum. The four other separations; 50 cm., 20 cm., 10 cm., and 5 cm.; were spaced approximately logarithmically between the largest separation and the smallest separation.

Chapter 3

INSTRUMENTATION

The Array

In the assembly designed to support the sensors, shown in Figure 1, all the members were 1" square aluminum tubing which had a very high resistance to torsion and to bending. The structure was stayed by guy wires fastened to several points. When setting up the array for a run, all arms and legs were made vertical or horizontal by adjusting the lengths of the guy wires. The characteristic vibration frequencies of each member of the assembly were different being dominantly near one or two cycles per second. Any vibration excited in an arm of the assembly tended to be damped out after about a cycle.

The hot wire anemometers were supported by clamps which could slide along the square tubing to attain any desired sensor separation. The susceptibility of the anemometer probe support to vibration was tested on the Mechanical Engineering Department vibrating machine. The characteristic vibration frequency of each support depended strongly on the precise position of the hot wire probe holder in the supporting clamp. Because vibrations were hard to excite and because the vibration frequencies would be different for each support it was not expected that vibrations would present a significant problem. Possible effects were looked for but were not detected in any of the data analyzed. The three dimensional sonic anemometer and the cup anemometer also used in the experiment were fastened to the horizontal cross-stream bar of the

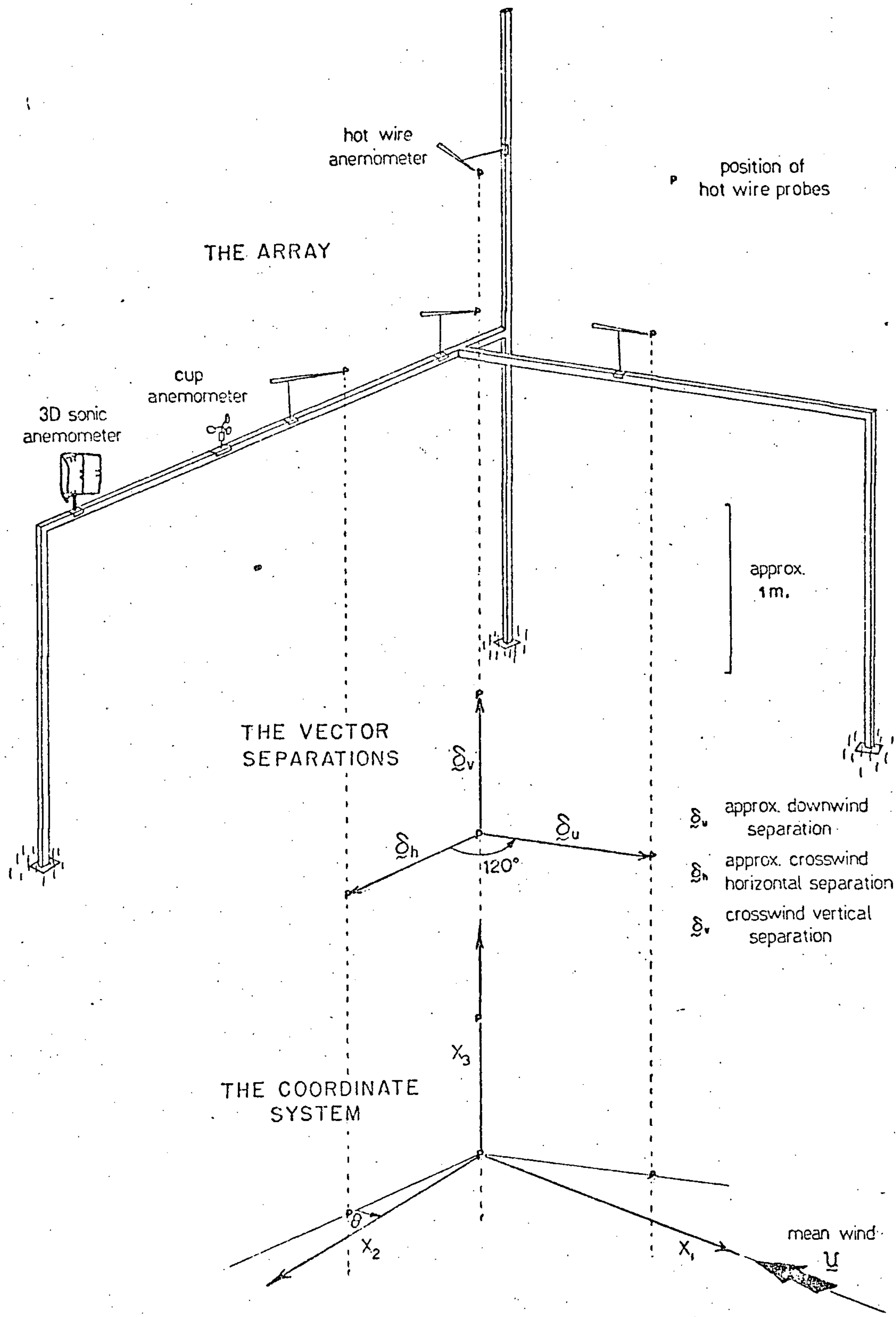

Figure 1: The Array, Vector Separations, and Coordinate System.

assembly in such a way that their sensors were centered at the same 2 m. level as the three lower hot wire anemometers.

The Hot Wire Anemometers

Four hot wire anemometers were used in this experiment to measure the cross spectra of downwind velocity fluctuations. The operating principle of hot wire anemometers depends on the cooling effect of the wind on a very fine piece of heated wire whose resistance depends on temperature. Hot wire anemometers have the two characteristics necessary to the present experiment, small sensor size and fast response. The particular sensors used had a size of about 1.5 mm. and the devices as a whole were adjusted to respond to velocity fluctuations up to at least 10,000 Hz.

The hot wire anemometers, which were Disa battery operated constant resistance types*, have a non linear response given by 'King's Law':

$$\xi^2 = A + B\sqrt{V} \tag{3.1}$$

where ξ is the output voltage, V is the instantaneous magnitude of the wind perpendicular to the sensing element and A and B are constants depending on the particular anemometer and on the temperature of the air. For low turbulence levels output voltage fluctuations, e, are linearly related to the first order to the downwind velocity fluctuations, u; the effect of the next order of response is examined in detail in the section on measurement error on page 27. The calibration constant for

---

* Electronics: Disa type Do55; Probes: Disa type 55A22.

the linear response of the hot wire anemometer was determined by matching the hot wire voltage spectra at low frequencies to velocity spectra observed using the sonic anemometer. The sonic anemometer, which responds to scales larger than about 1m., is a much better device for measuring absolute velocities because the operating levels of the hot wires are liable to change considerably due to age or to the adherence of specks of dust to the sensing element.

Because the hot wire anemometer operation depends on the cooling effect of the wind blowing past the wire, temperature variation in the air itself will affect the response. The contamination of the output signal by temperature fluctuations can be minimized by operating the hot wire at a sufficiently high temperature above ambient temperature. The magnitude of the temperature effect is estimated in the discussion on measurement error on page 30.

The Sonic Anemometer

The magnitudes and directions of the mean wind were measured using a three dimensional sonic anemometer mounted in a fixed position on the horizontal cross-stream arm of the array. The sonic anemometer measures wind velocity by comparing the times of flight of two sound pulses travelling in opposite directions over the same path. The difference in the two times is proportional to the component of the wind in the direction of the path. The instrument used senses components along such paths oriented so the three instantaneous velocity components; u, v, w; can be computed. In addition, by measuring the absolute sound velocity, the sonic anemometer will provide the instantaneous density fluctuation, ρ' or equivalently the virtual temperature fluctuation, T_V' (Lumley & Panofsky, 1964). Besides determining the vector mean wind the sonic was also used to determine the Reynold's stress, $\overline{uw}$; the turbulent density flux, $\overline{\rho' w}$; and the downstream velocity fluctuation spectra for use in calibrating the hot wire anemometers.

On the 'Kaijo Denki' sonic anemometer used, the sonic paths were each 20 cm. long so its response to velocity fluctuations falls off with scales decreasing from about 1 m.

The Cup Anemometer

A Kenkusho cup anemometer was used as a check on the mean wind speed measured by the sonic anemometer. Because the cup responds to wind magnitude, and because it tends to 'overspeed' in turbulent flow it is expected to register a higher wind speed than the sonic anemometer. A comparative study by Izumi and Barad (1970) indicated that cup mean wind speeds were on the average 10% higher than mean wind speeds in the same flow measured by a sonic anemometer.

Data Recording

The voltage fluctuations from the various velocity sensors were recorded in FM mode on magnetic tape using an Ampex FR1300 fourteen channel tape recorder. Altogether nine channels of information were recorded simultaneously. Prior to recording, the signals from the cup and the hot wire anemometers were passed through 'gain-offset' amplifiers to ensure satisfactory signal to noise levels in the recorded signals.

Chapter 4

OBSERVATIONS AND SOME RESULTS

The Site

The site used for the measurements was an abandonned air field near Ladner, B.C. which is essentially flat, horizontal and relatively free of obstructions making it ideal for the study. The array itself rested on grass about 15 cm. high. This grassy area extended at least 200 m. in the wind approach direction before being crossed by an asphalt runway. Beyond the runway the grass continued further for about 1 km. before it ended at a dike bordering the shores of Boundary Bay. Because the maximum height of the uppermost sensor was only 4 m. it could be safely assumed that the runway and the dike had negligible influence on the turbulence seen by any of the sensors.

The Wind Conditions

All the measurements were made on April 28, 1971 which was a cool overcast day. Six runs were made each at a different separation and of approximately one half hour duration; the statistics of the analyzed section of each run are listed in Table I. The wind remained remarkably uniform in magnitude and direction over the whole period of the observations so the data sections analyzed were rather arbitrarily taken from near the beginning of each run. In Table I, $\overline{U}$ is the average of the mean wind speeds given by the sonic and by the cup anemometer. The cup mean wind was consistently higher than the sonic mean wind by between 3% to 10%. The angle of the mean wind,

TABLE I

The Wind Conditions for the Analyzed Section of each Run

Run Identification (by separation)	Time of Run (P.S.T.)	Duration of Analyzed Section(sec)	k_1 range of analysis $(m)^{-1}$	$\overline{U}$ (m/sec)	$\overline{\theta}$	$\overline{u^2}$ (m^2/sec^2)	$\overline{wu}$ (m^2/sec^2)	z/L_v
δ = 180 cm.	13:59	1015	$6.02 \times 10^{-3} \rightarrow 1.91 \times 10$	6.60	11.0^o	1.15	0.326	-
δ = 50 cm.	15:16	254	$4.09 \times 10^{-3} \rightarrow 7.73 \times 10$	6.55	20.1^o	0.930	0.299	-0.015
δ = 20 cm.	12:17	127	$8.19 \times 10^{-3} \rightarrow 1.55 \times 10^2$	6.54	13.4^o	0.888	0.235	-0.027
δ = 10 cm.	10:36	63.5	$1.79 \times 10^{-2} \rightarrow 3.37 \times 10^2$	6.00	12.2^o	0.858	-	-
δ = 5 cm.	11:05	31.8	$2.98 \times 10^{-2} \rightarrow 5.69 \times 10^2$	7.21	12.2^o	1.01	-	-
δ = 2 cm.	16:50	15.9	$6.82 \times 10^{-2} \rightarrow 1.29 \times 10^3$	6.29	16.8^o	0.653	-	-

θ, as defined in Figure 1 is that obtained from the sonic anemometer. The wave number range used for the spectral analysis of the data is given by 'k_1 range'. The 'k_1 range' for each run is different because all the runs were digitized at different frequencies. Both $\overline{u^2}$, the variance of downstream velocity fluctuations, and $\overline{uw}$, the Reynold's stress, are calculated from the sonic data. The averages for both are over the duration of the data section analyzed. The density flux, $\overline{\rho' w}$, arises because of variations in density due both to humidity and to temperature. The ratio of the height, z, to the Monin-Obukhov length, L_V, (Lumley and Panofsky, 1964) is a measure of the buoyancy effects in the structure of the turbulence. This ratio was computed for two runs and is shown in Table I; the small values indicate that effects of buoyancy are negligible during the measurements.

The Sonic Anemometer Spectra

The sonic anemometer spectra, $k_1 \cdot \Phi_u(k_1)$, $k_1 \cdot \Phi_v(k_1)$ and $k_1 \cdot \Phi_w(k_1)$, computed by the analysis scheme of Appendix B, are plotted for three of the runs on a log-log scale against $k_1 z$ in Figure 2. At low wave numbers the 'u' spectrum has the most energy and the 'w' spectrum has the least. The '-2/3 slope' line on each of the graphs corresponds to the '$k_1^{-5/3}$' form in the spectra predicted for the inertial subrange. The 'u' spectrum attains this slope at values of $k_1 z$ around 2 but the 'v' and 'w' spectra do not until $k_1 z$ is approximately 5. At still higher wave numbers the 'v' and 'w' spectra roll-off due to the effects of using a 20 cm. sound path for the velocity measurements. The difference in the shapes between runs of the 'u' and 'v' spectra at high wave numbers is probably due to aliased electronic noise. None of the sonic spectra should be considered reliable much above $k_1 z = 10$.

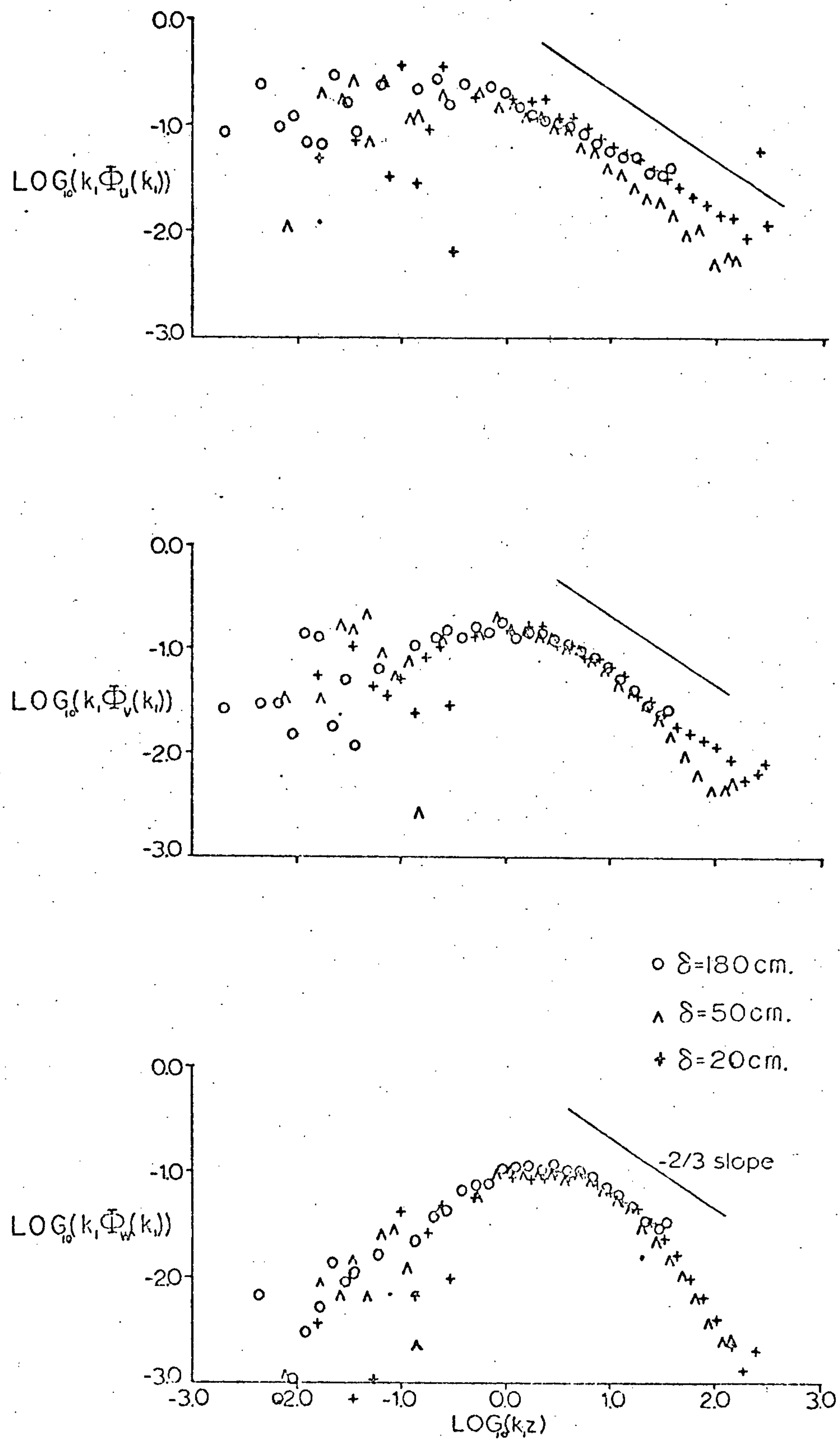

Figure 2: The Observed Sonic Anemometer Spectra for the Three Runs: δ = 180 cm., δ = 50 cm., δ = 20 cm.

The Hot Wire Anemometer Spectra

The hot wire anemometer spectra for a given run are all similar in shape to one another and to the 'u' spectra measured by the sonic anemometer in the wave number range where it gives reliable results. The hot wire anemometers were calibrated by matching the integrals of the low wave number voltage measured by the hot wires to the 'u' spectrum measured by the sonic anemometer (see Appendix B). Most of the difference between the details of the spectra of the hot wires for a given run appears to be due to random spatial variation of the turbulence; as the separation of the sensors decreases the details of the spectra become more similar. For the largest separation the upper hot wire at $z = 3.8$ m. seems to have slightly more energy at low wave numbers than the other three hot wires at $z = 2$ m. As one would expect, the two spectra from the hot wires separated approximately downstream of one another showed the most agreement in detail at all separations. When plotted together on a log-log graph versus k_1z the shapes of the spectra from the different runs fitted one another reasonably well as should be expected if the wind is statistically stationary. Figure 3 is a plot of such a composite spectrum obtained from the hot wire situated at the 'origin' of the array. As does the sonic 'u' spectrum the hot wire spectrum attains its inertial subrange form for $k_1z > 2$. It retains this form until $k_1z \sim 1000$ in the run analyzed to highest wave number, where it begins to roll-off due to dissipation effects.

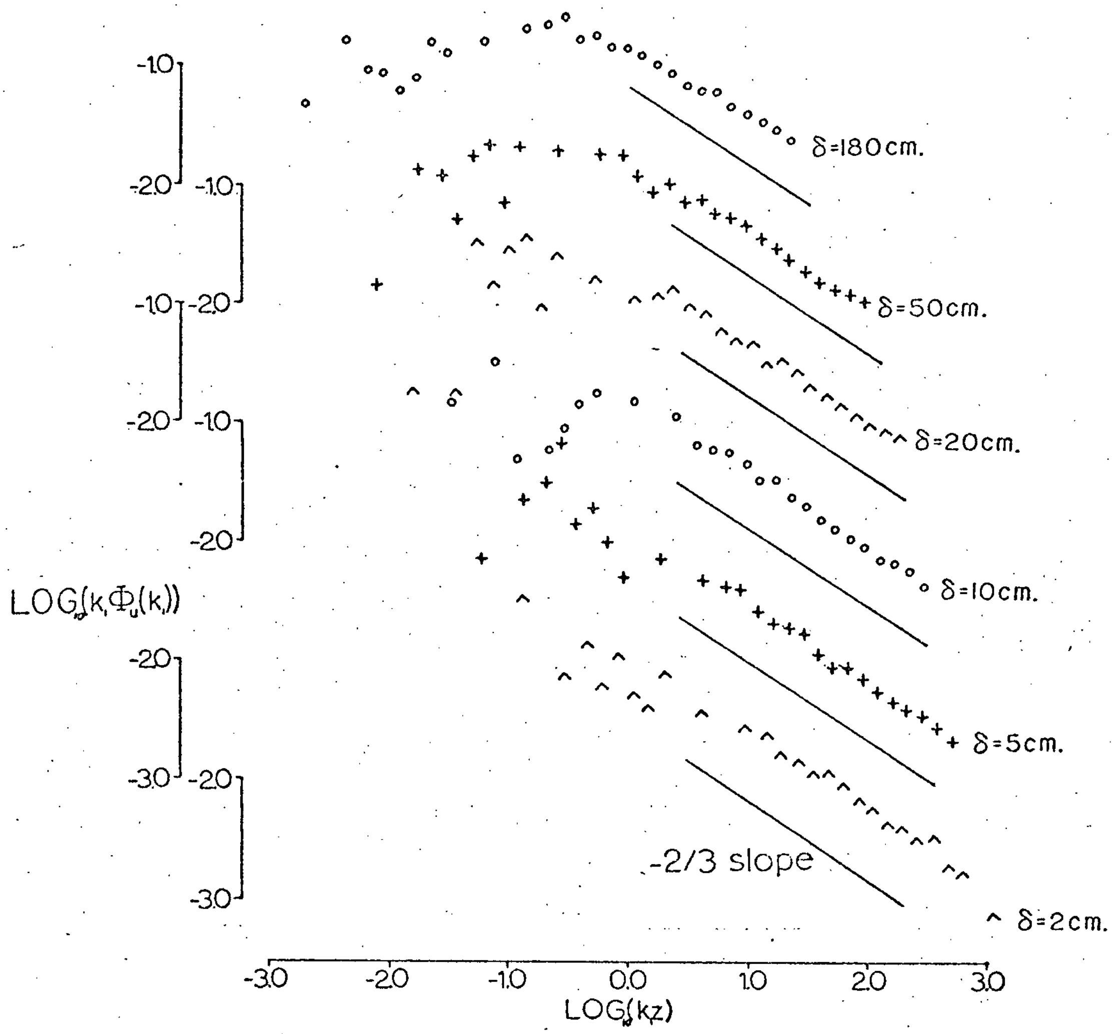

Figure 3: The Spectra Observed by the Hot Wire Anemometer at the Origin.

Chapter 5

THE THEORETICAL CROSS SPECTRA

The Determination of $E^T(k)$

The theoretical basis for predictions of cross spectra appropriate to isotropic turbulence obeying Taylor's hypothesis is outlined in Appendix A. The computational procedure for determining these theoretical cross spectra involved two steps. The first was the derivation of $E^T(k)$, the three-dimensional spectrum as defined in Appendix A, appropriate to the observed one-dimensional power spectra of downwind velocity fluctuations and the second was the computation, using the $E^T(k)$, of the various cross spectra for the different separations.

Providing the turbulence is isotropic and obeys Taylor's hypothesis then $E^T(k)$ is related to the one dimensional spectrum of downwind velocity fluctuations by Equation (A.14):

$$E^T(k) = \frac{k^3}{2} \frac{d}{dk} \left(\frac{1}{k} \frac{d\Phi_u^T(k)}{dk} \right)$$

Using the $\Phi_u^o(k_1)$ measured by the hot wire anemometers a theoretical $E^T(k)$ was to be estimated using the above relation. The measured spectra, $\Phi_u^o(k_1)$, are, however, a series of discrete estimates which can not be used directly in the equation for $E^T(k)$. To circumvent this difficulty analytic functions were fitted to the observed spectra. These analytic functions were the $\Phi_u^T(k)$ used in the equation to estimate $E^T(k)$. The analytic functions, $E^T(k)$, which resulted were then used for the subsequent computation of theoretical cross spectra.

To obtain an analytic form for $\Phi_u^T(k_1)$ a least squares fitting procedure was applied to the geometric means of the spectral estimates from each of the pair of hot wires for which the cross spectrum was to be computed. Each spectral estimate was weighted by the bandwidth over which the estimate was averaged. In a few cases where there were indications of significant noise as, for example, near the high frequency end of the spectrum for the 2 cm. separation where the effects of aliasing of a high frequency pick-up become noticeable, a zero weight was assigned to the estimate. Initially, an attempt was made to fit a function of polynomial form, or of a polynomial of logarithmic form to the complete hot wire spectrum produced by the computer program SIMPLØT (see Appendix B). In order to get reasonable fits over the whole spectrum it was necessary to go to rather higher order functions than would be easy to handle. By superimposing the spectra from the different separations each of which covers a different wave number range on a log-log plot one can obtain a view of the complete spectrum (see Figure 3). Over a large portion of the wave number range the shape of this composite spectrum appears linear which suggests a simple power law might be a good approximation to the spectrum in these regions. The spectrum at each separation was thus fitted according to (5.1) over this wave number range.

$$\Phi_u^T(k_1) = Ak_1^{\,B} \tag{5.1}$$

Here, A and B, the constants determine for each pair of hot wires at each separation, are listed in Table II. Figure 4 illustrates the spectral estimates which were used for this fitting and the slope of the respective fits at each separation for the pair of hot wires having the approximately downwind separation.

TABLE II

The Constants A and B for the Fitted Spectrum, Ak_1^B

Run Identification (by separation)	Approximately Downstream Separation		Approximately Horizontal Transverse Separation		Vertical Separation	
	A(M.K.S.)	B	A(M.K.S.)	B	A(M.K.S.)	B
δ = 180 cm.	0.935	-1.57	0.930	-1.56	0.840	-1.60
δ = 50 cm.	1.06	-1.63	1.03	-1.61	1.00	-1.63
δ = 20 cm.	1.16	-1.62	1.02	-1.60	1.12	-1.62
δ = 10 cm.	1.16	-1.65	1.07	-1.63	1.13	-1.64
δ = 5 cm.	1.16	-1.68	1.09	-1.66	1.14	-1.68
δ = 2 cm.	0.638	-1.56	0.591	-1.55	0.620	-1.56

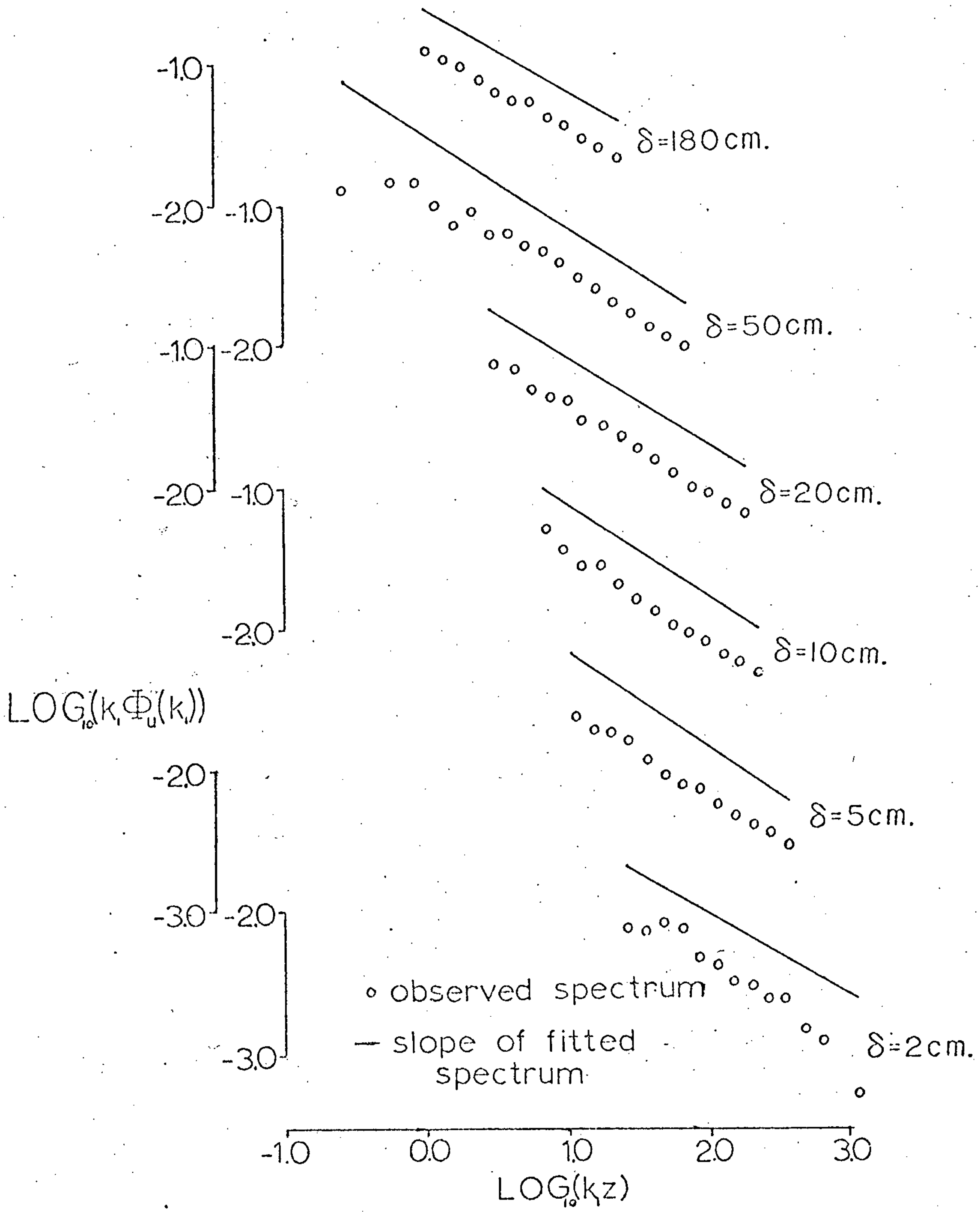

Figure 4: The Observed Hot Wire Spectral Estimates Used for Fitting and the Slopes of the Respective Fits.

The Computational Procedure

From the fitted forms, expressions for $E^T(k)$ were determined analytically as simple power law functions. On the assumption that an isotropic turbulence corresponds to the observed spectra, the theoretical cospectra, quadspectra, and coherences were evaluated using the Equations (A.11), (A.12) and (2.7):

$$Co^T(k_1,\underset{\sim}{\delta}) = \cos k_1\delta_1 \int_0^\infty\int_0^\infty \frac{E^T(k)}{\pi k^4}(k_2^2+k_3^2)\cos(k_2\delta_2+k_3\delta_3)\,dk_2\,dk_3$$

$$Qu^T(k_1,\underset{\sim}{\delta}) = \sin k_1\delta_1 \int_0^\infty\int_0^\infty \frac{E^T(k)}{\pi k^4}(k_2^2+k_3^2)\cos(k_2\delta_2+k_3\delta_3)\,dk_2\,dk_3$$

$$Coh^T(k_1,\underset{\sim}{\delta}) = \frac{\left[(Co^T)^2 + (Qu^T)^2\right]^{\frac{1}{2}}}{\Phi_u^T(k_1)}$$

where δ_1, δ_2, and δ_3 are cartesian component separations in the coordinate system defined by the observed direction of the mean wind. Because $E^T(k)$ is assumed to be of simple power law form, the above integrations can be converted to integrations over two other integration variables one of which can be performed analytically whereas the other can easily be evaluated numerically. The numerical integration was carried out using a Simpson's rule subroutine on the university's computer using a high enough upper wave number limit to ensure proper convergence. Theoretical cross spectra are plotted in Figures 6, 7, 8 and 9 with the observed cross spectra; these will be discussed later.

Although a realistic $E^T(k)$ like a realistic $\Phi^T(k)$ would roll-off at low and high wave numbers this was not accounted for in any of the theoretical cross spectra. Because the minimum value of $\underset{\sim}{k}$ is just $(k_1, 0, 0)$ in any integration the low wave number roll-off has no influence on the integration as long as k_1 is above the roll-off region.

On the other hand, the upper limits of integration extended into wave number regions where the high wave number roll-off might become significant. Judging by the slope of the observed spectra at the highest wave numbers, $E^T(k)$ might be expected to be truncated considerably by viscous dissipation effects at wave numbers, $\tilde{k}$, near 1000 m^{-1}. Using the upper integration limits of $k_2 = 1000\ m^{-1}$, and $k_3 = 1000\ m^{-1}$ the effect of the roll-off on the 2 cm. normalized cospectra and coherences was estimated. Compared to those cross spectra computed using the normal integration limits the cross-stream cospectra were altered by 0.01 or so near $k_1\delta = 10.0$ whereas the downstream coherence was increased by 0.04 near $k_1\delta = 10.0$. For wave numbers less than $k_1\delta = 3.0$ the downstream coherence was almost imperceptibly altered. For all the larger separations the effect on the cross spectra of the high wave number roll-off would be much less.

The Check On The Computational Procedure

The derivations and computational procedures for these calculations were checked by computing cospectra for both a purely downstream separation and a purely cross-stream separation which would result from a '$k^{-5/3}$' power spectrum. For a purely downstream separation it can easily be shown theoretically that the normalized cospectrum is given by the particularly simple form:

$$\frac{\overset{T}{Co}(k_1,\delta)}{\phi_u^T(k_1)} = \cos(k_1\delta) \tag{5.2}$$

The result obtained using the numerical procedure agreed with this within ± 0.005. The difference between the spectrum and the cospectrum when integrated with respect to wave number yields the value of the structure function for that particular separation. On dimensional grounds one predicts that in the inertial subrange the ratio of the cross-stream to downstream structure function should be 1.33 (Lumley and Panofsky, 1964). This ratio was obtained for structure functions estimated from the computed cospectra corresponding to the ideal '$k^{-5/3}$' form. That the downstream cospectrum and ratio of structure functions evaluated numerically from this form agree with the analytical predictions confirms that the expressions, (A.11) and (A.12), were correctly derived and that the numerical procedure is a correct one.

Chapter 6

MEASUREMENT ERRORS

Ideally, a sensor would respond linearly to downstream velocity fluctuations; in practice the response of hot wires is non-linear and they also respond somewhat to transverse velocity fluctuations and to temperature fluctuations. The computations of the theoretical cross spectra are subject to error due to uncertainty in the precise vector separation of the sensors and to variance associated with the estimate of a form representative of the observed downwind spectra. In the following each of the above effects is investigated.

The Effect of Non-Linearity of the Hot Wires on Observed Cross Spectra

In all the computation of observed cross spectra the hot wire anemometers were treated as if they had a voltage response, e, to small downwind fluctuations, u, given by:

$$e = cu \tag{6.1}$$

where c is a calibration constant. However the 'King's Law' response for the hot wires used is (3.1):

$$\xi^2 = A + B\sqrt{V_h}$$

where V_h is the total horizontal component of wind speed and ξ is the output voltage. Because the velocity fluctuations in the cross stream direction were small compared to the magnitude of the mean wind then V_h is nearly the instantaneous magnitude of the wind in the downstream direction. By solving (3.1) for V_h and expanding in a Taylor's series one obtains the second order response for the downstream fluctuations, u:

$$u = C\left(e + \tfrac{1}{2}\left(\frac{1}{\overline{\xi}} + \frac{2\overline{\xi}}{B\overline{V}_h^{\,\frac{1}{2}}}\right)e^2\right) \tag{6.2}$$

C is a constant depending on A, B, the mean voltage, $\overline{\xi}$, and the mean wind speed, $\overline{V}_h$. Using the constant B determined by a wind tunnel calibration of the hot wire a section of data was analyzed using both the linear calibration, (6.1), and the more correct non-linear calibration, (6.2). Figure 5c shows a comparison of the two analyses for a normalized downwind cospectrum for a 50 cm. separation. In the region of the drop-off the corrected (non-linear) calibration is seen to result in normalized cospectral estimates which are as much as 0.05 higher than the corresponding estimates obtained using the uncorrected (linear) calibration. The alteration to cross-stream cospectra using non-linear calibrations would be expected to be similar. Because the non-linear response affects large amplitude velocity fluctuations more than small amplitude fluctuations and because the large amplitude fluctuations tend to be at the lower wave numbers the cross spectra from the smaller separations, which cover higher wave number ranges, should be affected less by the non-linear response than those from the 50 cm. separation.

The Effect of Transverse Velocity Fluctuations on Observed Cross Spectra

In the experiment the hot wire anemometers respond to the instantaneous horizontal magnitude of the flow. As a result, the output voltage of the hot wire is somewhat dependent on the transverse horizontal velocity fluctuations, v. Using the 'King's Law' response equation (3.1) one can estimate that for small u and v the variance of the voltage will appear as:

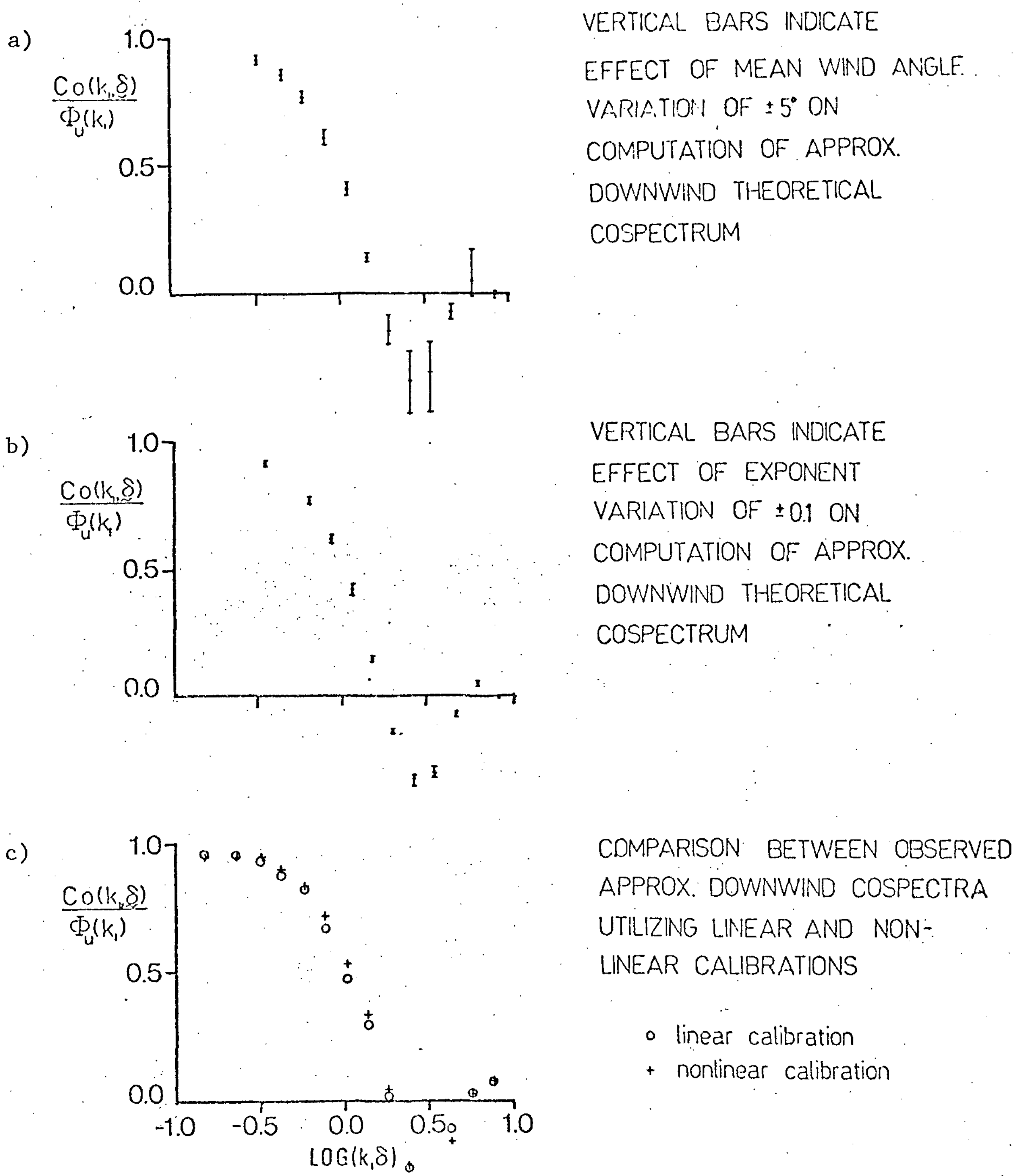

Figure 5: The Effect on Normalized Cospectra of Wind Angle Variation, Exponent Variation and Linear and Non Linear Hot Wire Calibrations.

$$\overline{e^2} \; \alpha \; \overline{u^2} + \frac{\overline{u^4}}{U^2} + \frac{\overline{v^4}}{U^2} \tag{6.3}$$

Both $\overline{u^2}$ and $\overline{v^2}$ were observed to be around 1 m^2/sec^2 and the mean wind speed, U, to be around 6m /sec, so that both $\frac{\overline{u^4}}{U^2}$ and $\frac{\overline{v^4}}{U^2}$ were about 0.03 $\overline{u^2}$. The term $\frac{\overline{u^4}}{U^2}$ arises because of the non-linear response of the type already discussed, but $\frac{\overline{v^4}}{U^2}$ is a measure of the increased variance resulting from the influence of transverse velocity fluctuations. The maximum magnitude of error in the spectra due to the latter effect is expected to be about the same as the 3% alteration to the variance; the alteration to the cross spectra normalized by the spectra would probably be less than this amount.

The Effect of Temperature Fluctuations on Observed Cross Spectra

Because the principle of operation of a hot wire anemometer depends on the cooling of a heated wire by the wind its output depends somewhat on air temperature fluctuations. This effect can be estimated from formulae given by Bearman (1970). Using a typical observed R.M.S. temperature fluctuation of 0.5°C, the hot wire operating temperature of 600°C as well as typical hot wire calibration constants, typical mean wind speeds and typical hot wire outputs for the experiment the temperature effect is expected to produce equivalent R.M.S. velocity fluctuations of about 0.006 m/sec. This is fairly small compared to the observed R.M.S. velocity fluctuations of around 1 m/sec.

The Statistical Reliability of Estimates

Even though the turbulence may be assumed to be stationary, as long as its averages are over a finite number of realizations of the flow, each estimate has a variance associated with its statistical nature. Jenkins and Watts (1968) derive expressions for the variance, σ^2, of the coherence estimators, $Coh(k_1,\underset{\sim}{\delta})$, under the assumption that the random process considered behaves like white noise:

$$\sigma^2_{Coh} \approx \frac{\{1-\left(Coh(k_1,\underset{\sim}{\delta})\right)^2\}}{\nu} \tag{6.4}$$

ν, the number of degrees of freedom of the estimate, is equal to twice the product of the number of estimates in the wave number band over which it is averaged and the number of data records over which it is averaged. Because the quadspectrum is relatively small, the cospectrum normalized by the spectrum is similar to the coherence [see (2.7)]. For a process of the type considered the cross spectral estimators are distributed approximately normally about the averages that would be obtained from an infinite number of realizations of the flow. The 68% confidence limits for a normal distribution are given by $\pm\,\sigma$; thus the expected error in the cospectra is approximately given by σ_{Coh}. In the region of maximum slope of the coherences and of the normalized cospectra (these features are discussed in the following sections and are shown in Figures 6, 7, 8 and 9) the expected variation of the estimates is around $\pm$ 0.05. σ_{Coh} is smaller both as the coherence goes to 1.0 at low wave numbers and as it approaches zero at high wave numbers where the bandwidth for each estimate increases. If the process is not completely stationary as was probably the case for the turbulence studied, the statistical variations of the observed cross spectral estimates would be expected to be somewhat larger than those predicted.

The Effect of Errors in Mean Wind Speed and Direction on the Theoretical Cross Spectra

The important parameters in the computation of theoretical cross spectra are the values of $k_1\delta$ and the direction of the mean wind with respect to the vector separations of the four sensors in the array. Inevitably there is some uncertainty in the exact position of each hot wire sensor on the array which introduces possible errors in both the magnitudes and directions of the separations. Because of errors in estimating the magnitude and direction of the mean wind using the sonic anemometer, the orientation and magnitude of the wind with respect to the array also has some doubt. Whereas the maximum error in $k_1\delta$ due to both effects is estimated to be ± 6% at most, the expected error in $k_1\delta$ is ± 3%. Likewise the maximum and probable error in the direction of the mean wind are estimated to be $\pm 5^{\circ}$ and $\pm 3^{\circ}$ respectively. The effect of introducing a change in the mean wind angle of $\pm 5^{\circ}$ in the computation of a cospectrum from an approximately downwind separation is shown in Figure 5a. The cross-stream cospectra are negligibly affected by mean wind direction changes of this size.

The Effect of Spectral Distortion on Theoretical Cross Spectra

Even though a low pass filter was used prior to digitizing the analog signals to help eliminate 'aliasing', some leakage of high wave number energy into the lower wave numbers of analysis did occur. Energy also leaks from low wave numbers to higher wave numbers due to the shape of the transfer function for a finite data record. Although the latter effect was corrected for prior to the plotting of the normalized cross spectra, the spectral fittings were made using uncorrected estimates.

The non-linearity in response of the hot wires discussed also tends to cause low wave number energy to appear at higher wave numbers. The combination of the three sources of distortion on the observed spectra causes errors in both the level, A, and in the exponent, B, of the fitted spectra, Ak_1^B. Even though the errors in level of each spectrum might be as large as + 15% in the worst case they produce no error in estimates of normalized cross spectra since both numerator and denominator are affected similarly. The exact exponent of the fitted spectrum does, however, alter the theoretical normalized cross spectra. Figure 5b illustrates that the effect of altering the exponent of the fitted spectrum by ± 0.1, the extreme maximum deviation expected, is to cause shifts in the values of the normalized cross spectra of about ± 0.02.

The Summary of Error Estimation

One can summarize the preceding by estimating the maximum expected difference between observed and theoretical normalized cross spectra due to error. The maximum error is evaluated by adding linearly the maximum deviations to the cross spectra expected at each separation arising from mean wind angle uncertainty, from uncertainty in $k_1\delta$, from non-linearity of the hot wires, from uncertainty in the exponent of the fitted spectrum and from the probable statistical fluctuations of the observed estimates. As the normalized cross spectra converge to zero at high wave numbers and as they converge to 1.0 at low wave numbers the error in the estimates should approach zero. The maximum error in the normalized cross spectral estimates is expected in the range of wave numbers in which the roll-off is steepest. In this region all observed normalized cospectral and coherence estimates should have statistical fluctuations of about $\pm$ 0.05. Also in the region of maximum slope the curves representing the theoretical and observed normalized cross spectra may be biased with respect to one another either up or down by $\pm$ 0.08 for the cross-stream cospectra and by $\pm$ 0.15 for the downstream coherences and cospectra.

Chapter 7

DISCUSSION OF RESULTS

The Comparison of Observed and Theoretical Cross Spectra

Figures 6, 7 and 8 illustrate the comparisons of the observed cospectra with those computed theoretically from the observed spectra assuming isotropy and Taylor's hypothesis. Each point on these plots is normalized; the observed cospectral densities are normalized by the observed spectral densities and the theoretical cospectral densities by the fitted spectrum. The abscissae on the plots are values of $\log_{10}(k_1\delta)$ where δ is the approximate magnitude of the vector separations for each run. Any power law behavior for the spectrum implies similarity of the normalized cospectra with respect to $k_1\delta$ for different runs if δ were the exact magnitude of the separations and if the angles between the mean wind direction and the vector separations were the same. Because the exact vector separations are used in their computations, the normalized theoretical cross spectra as plotted are only roughly similar from run to run. The representations of theoretical and observed cospectra differ in one important respect; whereas each theoretical estimate of cospectral density is a computation at a discrete value of k_1, the observed estimates represent an average over a band of wave numbers near k_1 (see Appendix B). Only for the first negative peak of the observed downstream cospectra (see Figure 8) where the curvature of the cospectral curve is relatively large should the effect of band averaging result in noticeable alterations to the observed cospectral estimates. The magnitudes of the observed estimates near this peak are expected to be reduced by no more than 10%.

Qualitatively, the theoretical and the observed cospectra are similar to one another for all separations. Both sets of cospectra decrease from the levels of the spectra at low values of $k_1\delta$ and tend to zero at higher values of $k_1\delta$. At intermediate values of $k_1\delta$ the observed approximately downstream cospectra oscillate about zero as do their theoretical counterparts.

Although normalized cross spectra will converge to 1.0 or to 0.0 at low or high values of $k_1\delta$ respectively, the shape and position of the cross spectral curve in its region of maximum slope is dependent on the structure of the turbulence. Using tolerances outlined in 'The Summary of Error Estimation' (see page 33) it is evident that there is generally quantitative agreement between the normalized observed and theoretical cross-stream cospectra in this region of maximum slope (see Figures 6 and 7); good agreement is evident for the 20 cm., 10 cm. and 5 cm. separations; marginal agreement is evident for the 50 cm. separation and there is definite disagreement for the 180 cm. separation. The observed cospectra for δ = 2 cm. agree well up to $\log_{10}(k_1\delta) \approx 0.5$; at higher wave numbers there was evidence of electronic noise due to the presence of the sonic anemometer on the array. The observed cospectral estimates for both cross-stream directions for δ = 180 cm. seem to be significantly lower than the theoretical estimates for $k_1\delta < 3$ or equivalently for $k_1 < 1.7\ m^{-1}$. Furthermore because low wave number observed cospectral estimates for δ = 50 cm. and δ = 20 cm. tend to be somewhat low for both cross-stream directions up to values of $k_1\delta$ corresponding to $k_1 \approx 2\ m^{-1}$ (The vertical arrows on Figures 6 and 7 indicate $k_1 = 2\ m^{-1}$) it would seem that the transition from disagreement to agreement of these cospectra occurs at $k_1 \approx 2\ m^{-1}$ or for $k_1 z \approx 4$.

None of the quadspectra are plotted. The observed cross-stream quadspectra which are expected to be near zero theoretically were scattered

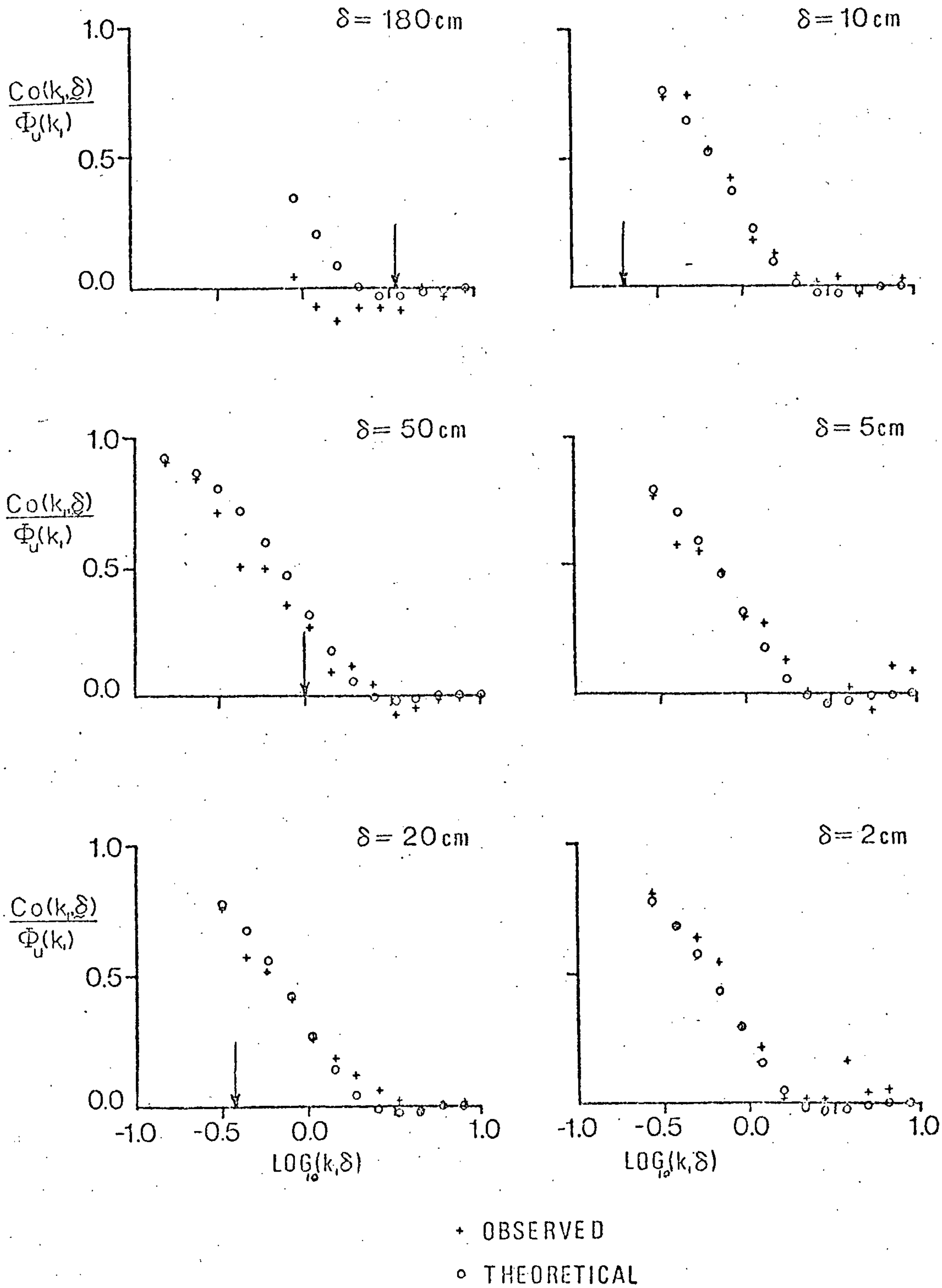

Figure 6: The Normalized, Observed and Theoretical Cospectra Obtained from the Approximately Horizontal Crosswind Separation. (The vertical arrow on each plot indicates $k_1 = 2\ m^{-1}$)

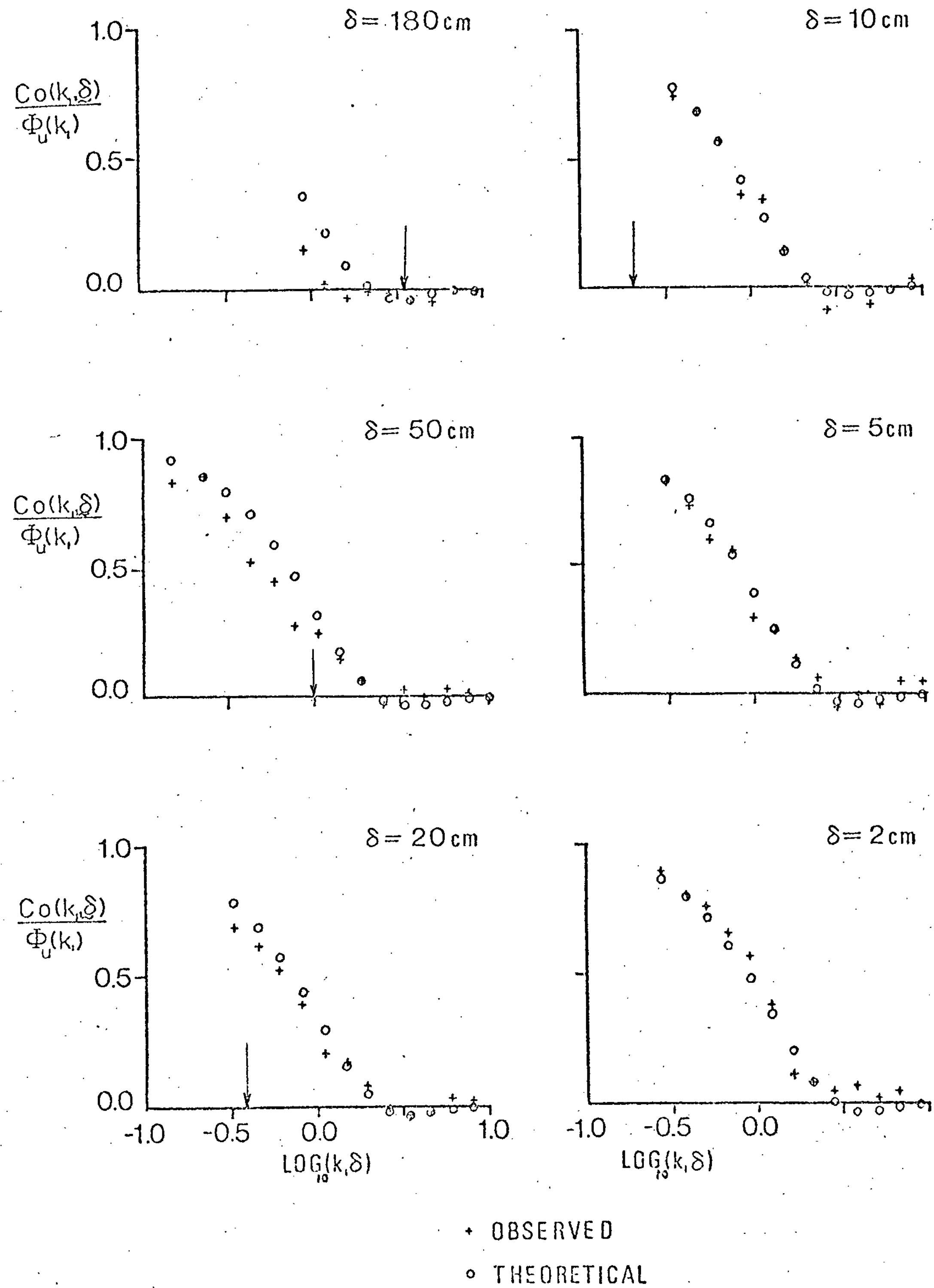

Figure 7: The Normalized, Observed and Theoretical Cospectra Obtained from the Vertical Separation.
(The vertical arrow on each plot indicates $k_1 = 2\ m^{-1}$)

about the theoretical values with what appeared to be random fluctuations of magnitude less than $\pm$ 0.1. Only the approximately downwind quadspectra had appreciable magnitudes, which is consistent with theoretical prediction.

The spectrum, cospectrum and quadspectrum together define the coherence [see equation (2.7)]. The cross-stream coherences are virtually identical with the cross-stream normalized cospectra which have already been discussed.

The approximately downstream normalized cospectra and coherences are shown plotted in Figures 8 and 9 respectively. The maximum expected errors in the region of the drop-off of the observed cospectrum and coherence are uniform shifts of all estimates of ± 0.15 and random fluctuations of estimates of average size ± 0.05. Up to the wave number at which the downstream cospectrum first crosses the zero axis all the observed cospectra agree with the theoretical predictions within experimental error. For this range of wave numbers the behavior of the downstream cospectrum is determined largely by the relative phase of the correlated energy at the two sensors. The observed phase, α_{obs}, is defined in (2.8):

$$\alpha_{obs} = \tan^{-1}\left(\frac{\overset{T}{Qu}(k_1,\underset{\sim}{\delta})}{\overset{T}{Co}(k_1,\underset{\sim}{\delta})}\right)$$

From (A.11) and A.12) the phase of the theoretical cross spectrum is seen to be simply $k_1\delta_1$ for a given wave number, k_1, and a given downwind component of separation, δ_1. Because from (B.2) k_1 is inversely proportional to the turbulence advection velocity, it is possible to define an effective advection velocity, U_{eff}, from the observed mean wind, U, from the theoretical phase, $k_1\delta_1$, and from the observed phase, α_{obs}:

$$U_{eff} = \frac{k_1\delta_1 U}{\alpha_{obs}}$$

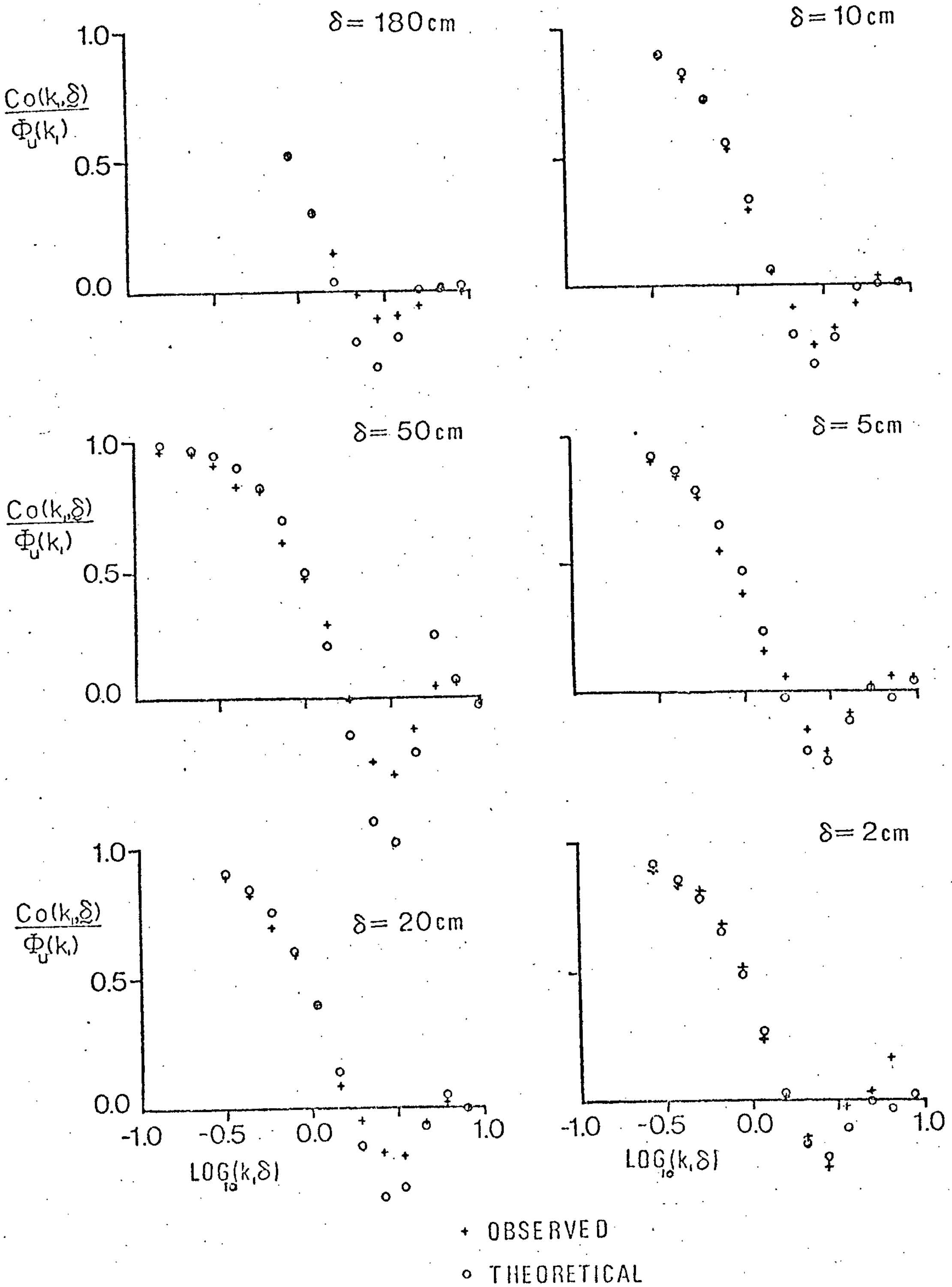

Figure 8: The Normalized, Observed and Theoretical Cospectra Obtained from the Approximately Downwind Separation.

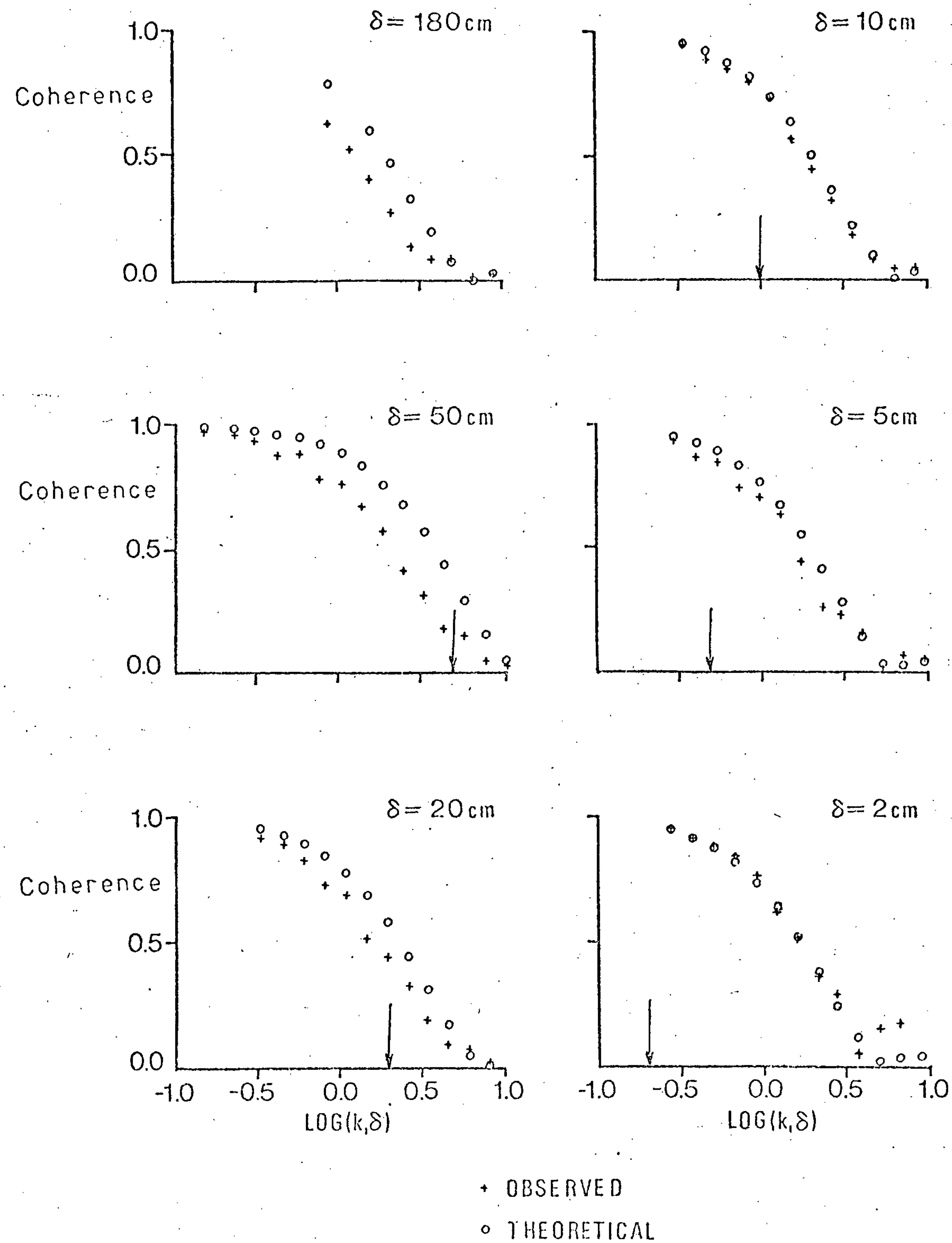

Figure 9: The Observed and Theoretical Coherences Obtained from the Approximately Downwind Separation.
(The vertical arrow on each plot indicate $k_1 = 10\ m^{-1}$)

The ratio, U_{eff}/U, was computed for the downwind pair of sensors. The average value of this ratio was 1.22 for wave numbers lower than 1.6 m^{-1} computed for the 1.8 m separation although for the same range of wave numbers from the 50 cm separation this average was 1.06. The average value of the ratio for all but the largest separation was 1.03. In view of the averages of the mean wind speed measured by the sonic and by the cup anemometer being up to 10% different from one another the difference of the average ratio from 1.00 is probably insignificant. Individual values of the ratio were scattered by up to $\pm$ 0.1 about the average but there was no significant trend in the values at increasing wave numbers.

On the other hand, the magnitude of the correlated energy is estimated by the coherence. The position of the maximum slope in the theoretical downstream coherence curves is determined primarily by the angle between the mean wind and the vector separation of the two velocity sensors; because this angle is smallest for δ = 50 cm. the coherence for this separation appears to 'hold up' to higher wave numbers than do those for the other separations. In fact, the coherence for a purely downstream separation would be 1.0 at all values of $k_1\delta$. In the region of maximum slope, the observed coherences from both the two largest downstream separations are too low to be explained by possible experimental error. These two coherences suggest that the theoretical and observed coherences do not agree for values of $k_1\delta$ corresponding to k_1 less than about 10 m^{-1}. (The vertical arrows on Figure 9 indicate k_1 = 10 m^{-1}). However, the observed coherence estimates for δ = 20 cm., although tending to be low, do agree within experimental error with the theoretical results for k_1 somewhat less than 10 m^{-1}. At smaller separations there appears to be quantitative agreement at all wave numbers except at the three highest ones on the $\delta = 2$ cm. plot where an electronic pick-up is evident. One can say that the coherence determination is too insensitive to establish at exactly what wave number the observed coherence and theoretical coherence agree, but agreement near $k_1 = 10\ m^{-1}$ or $k_1 z = 20$ seems the most likely.

The Anisotropic Models

Quantitative agreement occurs between the observed and theoretical cross spectra at approximately the same wave number for the two cross-stream separations but at a higher wave number for the downstream separations. This behavior suggests that a model of the turbulence which is axisymmetric about the downstream direction might describe the turbulence at wave numbers less than the isotropic range. Two such anisotropic models were considered; the first model has the axisymmetric energy density $E(\underset{\sim}{k}) = E(k)\cdot\cos\phi$ whereas the second also has an axisymmetric energy density given by $E(\underset{\sim}{k}) = E(k)\cdot(2 - \cos\phi)$. $E(k)$ is a scalar function of k and ϕ is the angle between the wave number $\underset{\sim}{k}$ and the k_1 axis so that the first model has a maximum energy density along the k_1 axis and the second a minimum. The normalized cospectra derived from these two models are plotted on Figure 10 together with the normalized cospectra from the isotropic model. The anisotropic model having the minimum of $E(\underset{\sim}{k})$ along the k_1 axis qualitatively describes the observations for low wave numbers; both the observed cospectral estimates and those computed from this model have smaller magnitudes than the corresponding isotropic estimates. It thus seems that some anisotropic model having a deficit of energy in the k_1 direction can explain the observations. The equation of continuity requires that $\nabla\cdot\underset{\sim}{u}=0$ or equivalently that $\underset{\sim}{k}\cdot\underset{\sim}{u}_{\underset{\sim}{k}}=0$ where u_k is the vector velocity arising from local integration about $\underset{\sim}{k}$ of the energy density

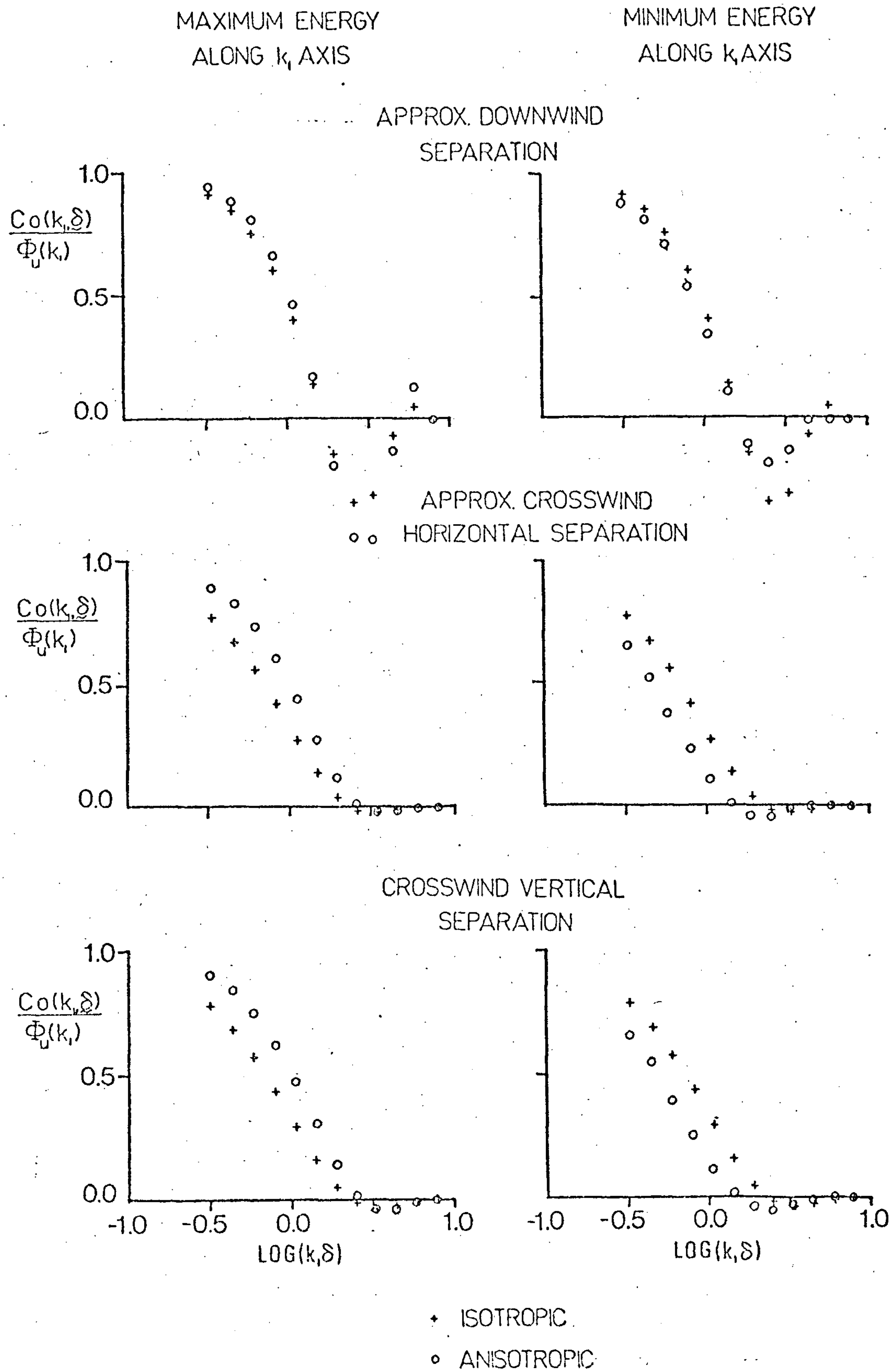

Figure 10: The Comparison of Normalized Cospectra Computed from Isotropic and from Two Anisotropic Models of the Turbulence

$E(\underset{\sim}{k})$. Thus, a model having a deficit of energy in the k_1 direction would predict an increment of energy in the downstream component of velocity, u. Ideally one could try more sophisticated anisotropic models to duplicate the observed cross spectra. In this experiment the possible error in the observed cross spectrum is too big to warrant the investigation of a reasonably accurate model of the actual turbulence.

Chapter 8

CONCLUSIONS

The purpose of this study was to obtain information on the approach to isotropy and on the applicability of Taylor's hypothesis in a high Reynold's number shear flow.

The observed cospectra and coherences within the accuracy of measurement are consistent with the assumptions of isotropy and of Taylor's hypothesis for $k_1 z > 20$.

At wave numbers between $k_1 z = 20$ and $k_1 z = 4$ the observed coherences for the downstream separation were lower than those predicted from the assumptions whereas the cospectra for both the vertical cross-stream and the horizontal cross-stream directions were within experimental error of the isotropic prediction. Furthermore the sonic 'v' and 'w' spectra are close to the expected inertial subrange shape, '$k_1^{-5/3}$', for $k_1 z > 5$ and the 'u' spectra measured by the sonic and the hot wire anemometers have this shape for $k_1 z > 2$. It thus appears that within the limits of accuracy of the experiment the turbulence is at least axisymmetric about the downstream direction for $k_1 z > 4$.

Coherences for all of the separation directions were lower than predicted on the isotropic assumption for $k_1 z > 4$. Failure of Taylor's hypothesis due to time evolution of the turbulence as it passes the pairs of velocity sensors would be expected to lower the coherences. An anisotropic model having an excess of energy spectral density distributed axisymmetrically about the k_1 axis also gives lower coherences than the isotropic model for the three separation directions. Such a model is consistent with the behaviour of the observed cross-stream cospectra in which there is an excess of energy in the 'u' component of velocity. Some anisotropy of this type and a partial failure of Taylor's hypothesis probably account for the observed nature of the cross spectra at low wave numbers.

Taylor's hypothesis involves both the assumptions that the time evolution of the turbulence as it is advected is negligible and that the turbulence is transported at the mean wind speed. The validity of the relation:

$$k_1 = \frac{2\pi f}{U}$$

is directly dependent on the latter assumption. The turbulence advection velocity computed from the relative phase of the coherent energy between the downstream pair of sensors does not appear to be significantly different from the wind velocity obtained directly from the anemometers for $k_1 > 1.6\ m^{-1}$ or for $k_1 z > 3$. For this range of wave numbers that part of Taylor's hypothesis relating measured frequency to downstream wave number appears to be valid.

In principle the method of comparing theoretical and observed cross spectra could be used to determine the quantitative details of the structure of the turbulence at different wave numbers. From four velocity sensors six different separations are possible for which cospectra can be computed. At each wave number it is possible to match the six observed cospectra and the spectrum with the cospectra and spectrum computed from a linear combination of seven different isotropic or anisotropic models of the turbulence. In order to determine the contribution of each model reasonably accurately the cospectra will have to be determined with less uncertainty than in the present study; the hot wire anemometers should be linearized, the wind angles and separations should be more precise, some account should be taken of the effect of 'v' fluctuations on the hot wire response and the statistical fluctuations of the estimates should be reduced by using longer data sections for example. If one were to use more than four velocity sensors then more separations would be possible and hence the turbulence could be modelled more exactly.

BIBLIOGRAPHY

Bearman, P.W. (1970) Corrections for the Effect of Ambient Temperature Drift on Hot-wire Measurements in Incompressible Flow. Disa Information 11, pp. 25-30.

Blackman, R.B. and J.W. Tukey (1958) The Measurement of Power Spectra. Dover Publications, Inc., New York; 190 pps.

Grant, H.L., R.W. Stewart and A. Moillet (1962) Turbulence Spectra from a Tidal Channel. J. Fluid Mech. 12, pp. 241-268.

Hinze, J.O. (1959) Turbulence. McGraw-Hill Book Co., New York; 586 pps.

I.E.E.E. Transactions on Audio and Electroacoustics, Special issue on Fast Fourier Transform and its application to digital filtering and spectral analysis. June 1967, Vol. AU15, No. 2.

Izumi, Y. and M.L. Barad (1970) Wind Speeds as Measured by Cup and Sonic Anemometers and Influenced by Tower Structure. J. Applied Met. 9, pp. 851-856.

Jenkins, G.M. and D.G. Watts (1968) Spectral Analysis and Its Applications. Holden-Day, San Francisco; 525 pps.

Kolmogoroff, A.N. (1941) The Local Structure of Turbulence in Incompressible Viscous Fluid For Very Large Reynold's Numbers, in Turbulence. Interscience Publishers, New York, pp. 151-155.

Lin, C.C. (1953) On Taylor's Hypothesis and the Acceleration Terms in the Navier-Stokes Equations. Quart. J. of Applied Math, 4, pp. 295-306.

Lumley, J.L. and H.A. Panofsky (1964) The Structure of Atmospheric Turbulence. Interscience Publishers, New York; 239 pps.

Pond, S., R.W. Stewart and R.W. Burling (1963) Turbulence Spectra In the Wind Over Waves. J. Atmos. Sci., 20, pp. 319-324.

Taylor, G.I. (1938) The Spectrum of Turbulence, in Turbulence. Interscience Publishers, New York, pp. 100-114.

Van Atta, G.W. and W.Y. Chen (1970) Structure Functions of Turbulence In the Atmospheric Boundary Layer Over the Ocean. J. Fluid Mech., 44, pp. 145-159.

Weiler, H.S. and R.W. Burling (1967) Direct Measurement of Stress and Spectra of Turbulence In the Boundary Layer Over the Sea. J. Atmos. Sci., 24, pp. 653-664.

APPENDIX A

THE DERIVATION OF THEORETICAL CROSS SPECTRA

The cross spectra $Cr_{ij}^{(n)}(\underset{\sim}{k},\underset{\sim}{\delta})$ are defined by:

$$Cr_{ij}^{(n)}(\underset{\sim}{k},\underset{\sim}{\delta}) = \frac{1}{(2\pi)^3}\int_{-\infty}^{\infty} \overline{u_i^{(n)}(\underset{\sim}{r},t)u_j^{(n)}(\underset{\sim}{r}+\underset{\sim}{\delta}+\underset{\sim}{x},t)}^{\underset{\sim}{r},t}\, e^{-i\underset{\sim}{k}\cdot\underset{\sim}{x}}d\underset{\sim}{x} \qquad (A.1)$$

We define the theoretical cross spectra $Cr_{ij}^{T}(\underset{\sim}{k},\underset{\sim}{\delta})$ as estimates of the cross spectra, $Cr_{ij}^{(n)}(\underset{\sim}{k},\underset{\sim}{\delta})$, smoothed according to (2.3) that would be obtained if the turbulence was stationary, isotropic and incompressible:

$$Cr_{ij}^{T}(\underset{\sim}{k},\underset{\sim}{\delta}) = \left\langle \frac{1}{(2\pi)^3}\int_{-\infty}^{\infty} \overline{u_i^{(n)}(\underset{\sim}{r},t)u_j^{(n)}(\underset{\sim}{r}+\underset{\sim}{\delta}+\underset{\sim}{x},t)}^{\underset{\sim}{r},t}\, e^{-i\underset{\sim}{k}\cdot\underset{\sim}{x}}d\underset{\sim}{x} \right\rangle_{n=1,\infty}$$

$$= \frac{1}{(2\pi)^3}\int_{-\infty}^{\infty} \left\langle \overline{u_i^{(n)}(\underset{\sim}{r},t)u_j^{(n)}(\underset{\sim}{r}+\underset{\sim}{\delta}+\underset{\sim}{x},t)}^{\underset{\sim}{r},t} \right\rangle_{n=1,\infty} e^{-k\cdot\underset{\sim}{x}}d\underset{\sim}{x} \qquad (A.2)$$

Likewise using (2.1) we can define an average of the product of velocity components in terms of the smoothed spectral tensor, $\Phi_{ij}^{T}(\underset{\sim}{k},\underset{\sim}{\delta})$:

$$\left\langle \overline{u_i^{(n)}(\underset{\sim}{r},t)u_j^{(n)}(\underset{\sim}{r}+\delta,t)}^{\underset{\sim}{r},t} \right\rangle_{n=1,\infty} = \int_{-\infty}^{\infty} \Phi_{ij}^{T}(\underset{\sim}{k})e^{i\underset{\sim}{k}\cdot\underset{\sim}{\delta}}d\underset{\sim}{k} \qquad (A.3)$$

substituting in (A.3) using (A.2) we have:

$$Cr_{ij}^{T}(\underset{\sim}{k},\underset{\sim}{\delta}) = \frac{1}{(2\pi)^3}\int_{-\infty}^{\infty}\left[\int_{-\infty}^{\infty} e^{i\underset{\sim}{k}'\cdot(\underset{\sim}{\delta}+\underset{\sim}{x})}\Phi_{ij}^{T}(\underset{\sim}{k}')d\underset{\sim}{k}'\right]e^{-i\underset{\sim}{k}\cdot\underset{\sim}{x}}d\underset{\sim}{x}\ . \qquad (A.4)$$

Assuming the functions are all well behaved one can switch the integration order in (A.4):

$$Cr_{ij}^{T}(\underset{\sim}{k},\underset{\sim}{\delta}) = \frac{1}{(2\pi)^3}\int_{-\infty}^{\infty}\left[\int_{-\infty}^{\infty} e^{i\underset{\sim}{x}\cdot(\underset{\sim}{k}'-\underset{\sim}{k})}d\underset{\sim}{x}\right]\Phi_{ij}^{T}(\underset{\sim}{k}')e^{i\underset{\sim}{k}\cdot\underset{\sim}{\delta}}d\underset{\sim}{k}' \qquad (A.5)$$

But:

$$\int_{-\infty}^{\infty} e^{i\underset{\sim}{x}\cdot(\underset{\sim}{k}'-\underset{\sim}{k})} d\underset{\sim}{x} = (2\pi)^3 \delta(\underset{\sim}{k}'-\underset{\sim}{k}) \tag{A.6}$$

where $\delta(\underset{\sim}{k}'-\underset{\sim}{k})$ is the Khrönecker delta function

Hence:

$$Cr^T_{ij}(\underset{\sim}{k},\underset{\sim}{\delta}) = \int_{-\infty}^{\infty} \delta(\underset{\sim}{k}'-\underset{\sim}{k})\Phi^T_{ij}(k')e^{i\underset{\sim}{k}'\cdot\underset{\sim}{\delta}}d\underset{\sim}{k}' = e^{i\underset{\sim}{k}\cdot\underset{\sim}{\delta}}\Phi^T_{ij}(\underset{\sim}{k}) \tag{A.7}$$

The cross spectra which were observed were the one dimensional cross spectra of downstream velocity fluctuations, $Cr^O_{11}(k_1,\underset{\sim}{\delta})$, in which the total contribution from all wave numbers is expressed in terms of the component, k_1, of wave number. The theoretical equivalent to this, $Cr^T_{11}(k_1,\underset{\sim}{\delta})$, can be computed from the general three dimensional cross spectrum, $Cr^T_{11}(\underset{\sim}{k},\underset{\sim}{\delta})$, by integrating it over all values of k_2 and k_3.

Hence:

$$Cr^T_{11}(k_1,\underset{\sim}{\delta}) = \int_{-\infty}^{\infty}\int_{-\infty}^{\infty} Cr^T_{11}(\underset{\sim}{k},\underset{\sim}{\delta})\,dk_2dk_3$$

$$= \int_{-\infty}^{\infty}\int_{-\infty}^{\infty} \Phi^T_{11}(\underset{\sim}{k},\underset{\sim}{\delta})e^{i\underset{\sim}{k}\cdot\underset{\sim}{\delta}}dk_2dk_3 \tag{A.8}$$

For isotropic incompressible turbulence the tensor, $\Phi^T_{ij}(\underset{\sim}{k},\underset{\sim}{\delta})$, can be expressed in terms of a single scalar function of k; $E^T(k)$: (Hinze, 1959).

$$\Phi^T_{ij}(\underset{\sim}{k}) = \frac{E^T(k)}{4\pi k^4}\,(k^2\delta_{ij}-k_ik_j) \tag{A.9}$$

The integral, (A.8), then becomes:

$$Cr^T_{11}(k_1,\underset{\sim}{\delta}) = \int_{-\infty}^{\infty}\int_{-\infty}^{\infty} \frac{E^T(k)}{4\pi k^2}\left(1-\frac{{k_1}^2}{k^2}\right)e^{i\underset{\sim}{k}\cdot\underset{\sim}{\delta}}\,dk_2dk_3 \tag{A.10}$$

The theoretical cospectrum, $\overset{T}{Co}(k_1,\underset{\sim}{\delta})$, and the theoretical quadspectrum, $\overset{T}{Qu}(k_1,\underset{\sim}{\delta})$, are the real and imaginary parts respectively of $Cr^T_{11}(k_1,\underset{\sim}{\delta})$. Noting that parts of the integral, (A.10), involving $\sin(k_2\delta_2+k_3\delta_3)$ are antisymmetric about $(k_2,k_3) = (0,0)$ and that the cosine function is symmetric about this point, the integration can be done over positive values of k_2 and k_3:

$$\overset{T}{Co}(k_1,\underset{\sim}{\delta}) = \cos k_1\delta_1 \int_0^\infty \int_0^\infty \frac{E^T(k)}{\pi k^2} \left(1-\frac{k_1^2}{k^2}\right) \cos(k_2\delta_2+k_3\delta_3)\,dk_2\,dk_3 \qquad (A.11)$$

$$\overset{T}{Qu}(k_1,\underset{\sim}{\delta}) = \sin k_1\delta_1 \int_0^\infty \int_0^\infty \frac{E^T(k)}{\pi k^2} \left(1-\frac{k_1^2}{k^2}\right) \cos(k_2\delta_2+k_3\delta_3)\,dk_2\,dk_3 \qquad (A.12)$$

If the separation, $\underset{\sim}{\delta}$, is zero then the one dimensional cospectrum is just the one dimensional spectrum $\Phi^T_u(k_1)$

$$\Phi^T_u(k_1) = \int_0^\infty \int_0^\infty \frac{E^T(k)}{\pi k^2} \left(1-\frac{k_1^2}{k^2}\right) dk_2\,dk_3 \qquad (A.13)$$

From (A.13) we can obtain $E^T(k)$ in terms of $\Phi^T_u(k_1)$

$$E^T(k) = \frac{k^3}{2}\frac{d}{dk}\left(\frac{1}{k}\frac{d\Phi^T_u(k)}{dk}\right) \qquad (A.14)$$

In this study the $\Phi^T_u(k_1)$ used to compute $E^T(k)$ are analytic functions fitted to the observed spectral estimates, $\Phi^O_{u'}(k_1)$.

APPENDIX B

THE OBSERVED CROSS SPECTRA

The Theoretical Basis

In this experiment velocity fluctuations were recorded as a function of time at four stationary sensors. The analysis of the data was carried out on velocities sampled at discrete time intervals, Δt, for a total record duration of $N\Delta t$, where N is the number of samples in the record. The cross spectra computed from the observed values of $u_i^{(n)}(\underset{\sim}{r},t)$ and $u_j^{(n)}(\underset{\sim}{r}+\underset{\sim}{\delta},t+T)$ sampling the n^{th} realization of the flow can only be obtained at the discrete frequencies; $f = 0, \frac{1}{M}, \frac{2}{M}, \frac{3}{M}, \ldots, \frac{N}{2M}$:

$$Cr'_{ij}(f\,,\underset{\sim}{\delta}) = \frac{1}{M}\int_{-M/2}^{M/2} \overline{u_i^{(n)}(\underset{\sim}{r},t)u_j^{(n)}(\underset{\sim}{r}+\underset{\sim}{\delta},t+T)}^{M} e^{-i2\pi fT}dT \qquad (B.1)$$

The velocity product average can only be taken over the time duration of the record, M. Provided the turbulence is stationary in space and time $Cr'_{ij}(f,\underset{\sim}{\delta})$ is not a function of $\underset{\sim}{r}$. Under Taylor's hypothesis (Taylor, 1938) the turbulence is assumed to be nearly 'frozen' in time as it is swept past a stationary sensor at a constant rate so the temporal velocity variations seen at the sensor are due only to spatial variations in the velocity along the line of the mean velocity. A cross spectral component having frequency, f, is then equivalent to the one dimensional cross spectral component having downstream wave number, k_1, where:

$$k_1 = \frac{2\pi f}{U} \qquad (B.2)$$

Thus:

$$Cr'_{ij}(k_1,\underset{\sim}{\delta}) = \frac{1}{M}\int_{-M/2}^{M/2} \overline{u_i^{(n)}(\underset{\sim}{r},t)u_j^{(n)}(\underset{\sim}{r}+\underset{\sim}{\delta},t+T)}^{M} e^{ik_1UT}dT \tag{B.3}$$

In practice the estimates of $Cr'_{ij}(k_1,\underset{\sim}{\delta})$ were not evaluated according to (B.3). Rather, a Fast Fourier Transform (I.E.E.E. Transactions, Vol. 15, 1967) was used to evaluate the complex Fourier coefficients, A'+iB', for $u_i^{(n)}(\underset{\sim}{r},t)$ and $u_j^{(n)}(\underset{\sim}{r}+\underset{\sim}{\delta},t+T)$:

$$A'_i(k_1,\underset{\sim}{r})+iB'_i(k_1,\underset{\sim}{r}) = \frac{1}{M}\int_{-M/2}^{M/2} u_i^{(n)}(\underset{\sim}{r},t)e^{ik_1Ut}dt \tag{B.4}$$

$$A'_j(k_1,\underset{\sim}{r}+\underset{\sim}{\delta})+iB'_j(k_1,\underset{\sim}{r}+\underset{\sim}{\delta}) = \frac{1}{M}\int_{-M/2}^{M/2} u_j^{(n)}(\underset{\sim}{r}+\underset{\sim}{\delta},t)e^{ik_1Ut}dt \tag{B.5}$$

The estimated cross spectra, Cr'_{ij}, are obtained from combinations of the coefficients in (B.4) and (B.5).

$$Cr'_{ij}(k_1,\underset{\sim}{\delta}) = A'_iA'_j+B'_iB'_j+i(A'_jB'_i+A'_iB'_j) \tag{B.6}$$

These estimates are exactly equivalent to those that would be computed by (B.3). Just as (B.1) can be evaluated at discrete frequencies only so (B.3), (B.4), (B.5) and (B.6) are defined at the discrete wave numbers; $k_1 = 0, \frac{2\pi}{MU}, \frac{4\pi}{MU}, \ldots, \frac{\pi N}{MU}$.

Because the $Cr'_{ij}(k_1,\underset{\sim}{\delta})$ are based on finite data records of duration, M, they are modified from the cross spectra, $Cr_{ij}^{(n)}(k_1,\underset{\sim}{\delta})$, computed from infinitely long records. The ensemble average of $Cr'_{ij}(k_1,\underset{\sim}{\delta})$ is related to the ensemble average of $Cr_{ij}^{(n)}(k_1,\underset{\sim}{\delta})$ by:

$$\left\langle Cr'_{ij}(k_1,\underset{\sim}{\delta})\right\rangle_{n=1,\infty} = \left\langle Cr^{(n)}_{ij}(k_1,\underset{\sim}{\delta})\right\rangle_{n=1,\infty}$$

$$+\left\langle \int_0^\infty \frac{Cr^{(n)}_{ij}(k'_1,\underset{\sim}{\delta})\,2U^2}{(k_1-k'_1)^2M} \left[1-\cos\left((k_1-k'_1)\frac{M}{U}\right)\right] dk_1 \right\rangle_{n=1,\infty} \tag{B.7}$$

Although each of the spectral estimators, $\left\langle Cr'_{ij}(k_1,\underset{\sim}{\delta})\right\rangle_{n=1,\infty}$, is made up mostly of energy from k'_1 near to k_1, the estimator has small contributions from all wave numbers of $\left\langle Cr^{(n)}_{ij}(k_1,\underset{\sim}{\delta})\right\rangle_{n=1,\infty}$. In the observed cross spectra it was found that there was a sufficient preponderance of energy at low wave numbers so that according to (B.7), the $\left\langle Cr'_{ij}(k_1,\underset{\sim}{\delta})\right\rangle_{n=1,\infty}$ would be significantly modified at high wave numbers. Provided that most of the contribution to the second term on the right in (B.7) comes from k'_1 less than k_ℓ and provided that one only considers corrections to estimates for which $k_1 >> k_\ell$ then this term can be simplified:

$$\left\langle \int_0^\infty \frac{Cr^{(n)}_{ij}(k'_1,\underset{\sim}{\delta})\,2U}{(k-k')^2M} \left[1-\cos\left((k_1-k'_1)\frac{M}{U}\right)\right] dk \right\rangle_{n=1,\infty} \approx$$

$$\int_0^{k_\ell} \left\langle Cr^{(n)}_{ij}(k'_1,\underset{\sim}{\delta})\right\rangle \frac{2U^2}{Mk_1^2} \left[1-\cos\left((k-k')\frac{M}{U}\right)\right] dk_1 \tag{B.8}$$

The integral on the right in (B.8) can be approximated as a sum over the observed low wave number cross spectral estimates, $Cr'_{ij}(k_1,\underset{\sim}{\delta})$:

$$\int_0^{k_\ell} \left\langle Cr^{(n)}_{ij}(k'_1,\underset{\sim}{\delta})\right\rangle \frac{2U^2}{Mk_1^2} \left[1-\cos\left((k_1-k'_1)\frac{M}{U}\right)\right] dk_1 \approx$$

$$\left(\frac{1}{k_1^2}\right) \sum_{k'_1=0}^{k_\ell} Cr'_{ij}(k'_1,\underset{\sim}{\delta}) \frac{2U^2}{M} \left[1-\cos\left((k_1-k'_1)\frac{M}{U}\right)\right] \Delta k'_1 \tag{B.9}$$

where $\Delta k_1'$ is the wave number bandwidth over which the estimate $Cr_{ij}'(k_1', \underset{\sim}{\delta})$ is averaged. The quantity under the summation in (B.9) is the constant, P_{ij}, for the given run. Thus (B.7) becomes:

$$\left\langle Cr_{ij}'(k_1, \underset{\sim}{\delta}) \right\rangle_{n=1,\infty} \approx \left\langle Cr_{ij}^{(n)}(k_1, \underset{\sim}{\delta}) \right\rangle_{n=1,\infty} + \frac{P_{ij}}{k_1^2} \tag{B.10}$$

In practice only the finite number of data records, L, were analyzed so that the observed cross spectra, $Cr_{ij}^{o}(k_1, \underset{\sim}{\delta})$, which were corrected for the spectral leakage term, $\frac{P_{ij}}{k_1^2}$, were given by:

$$Cr_{ij}^{o}(k_1, \underset{\sim}{\delta}) = \left\langle Cr_{ij}'(k_1, \underset{\sim}{\delta}) \right\rangle_{n=1,L} - \frac{P_{ij}}{k_1^2} \tag{B.11}$$

Because they are based on an average over a finite number of data records the cross spectral estimators, $Cr_{ij}^{o}(k_1, \underset{\sim}{\delta})$, will show statistical fluctuations about the smooth cross spectra, $\left\langle Cr_{ij}^{(n)}(k_1, \underset{\sim}{\delta}) \right\rangle_{n=1,\infty}$. The variance of $Cr_{ij}^{o}(k_1, \underset{\sim}{\delta})$ is reduced further in this study by averaging the estimates over bandwidth as well as over data records.

The Computation of Observed Cross Spectra

The analysis routine which produced the various cross spectra from the raw data tape is outlined in Figure 11. Most of the analysis was done on the University's I.B.M. 360 computer using computer programs developed by students at the Institute of Oceanography. Each step of the analysis procedure is elaborated in the following.

Digitization

The process of rewriting the analogue data tape in digital form is called digitization. The digital tape produced is obtained by sampling the analogue voltage at a constant digitization frequency.

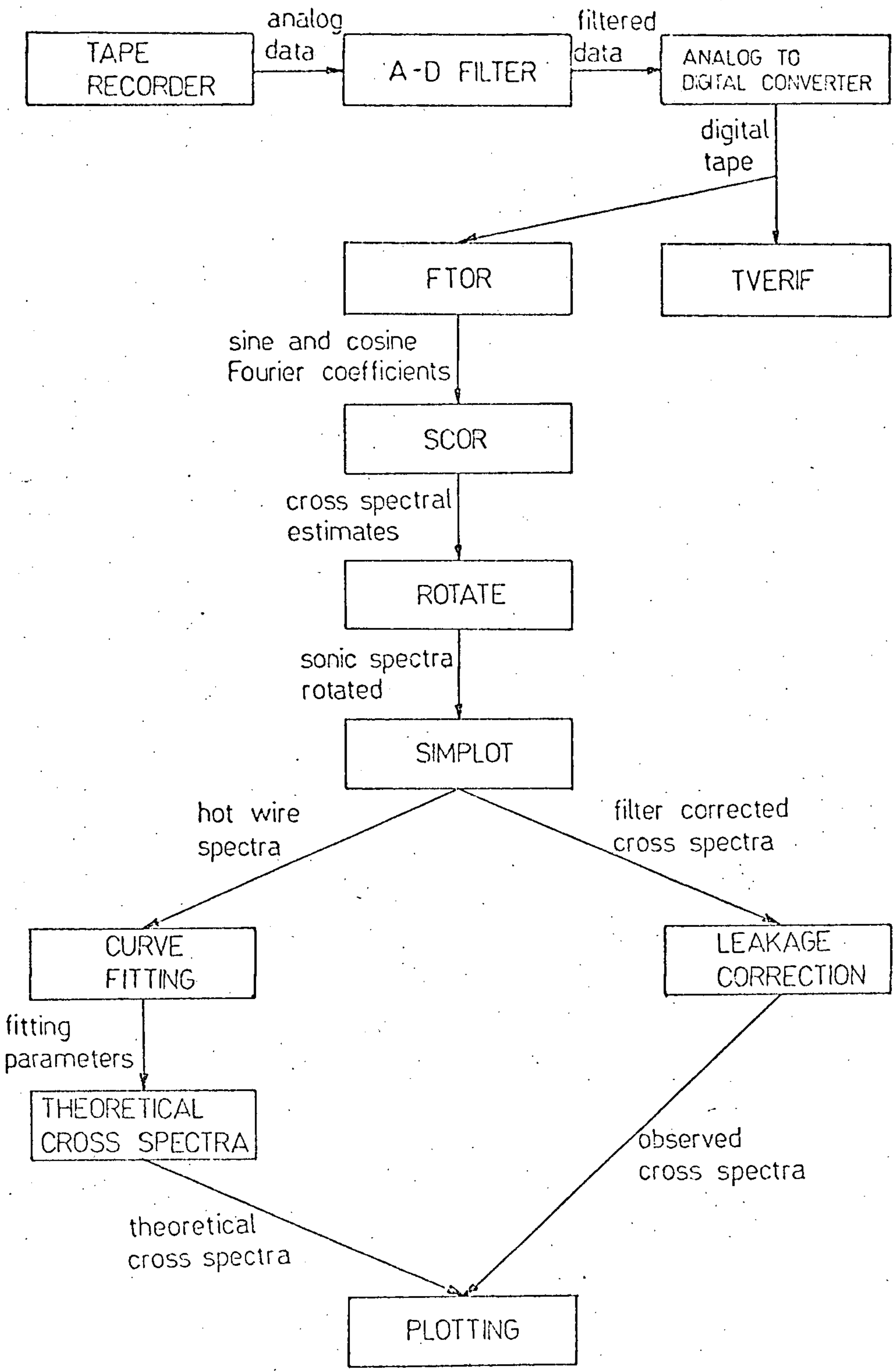

Figure 11: The Data Analysis Scheme.

The highest frequency at which energy can appear in the spectral analysis of such a digital tape is the Nyquist frequency, ω_N, equal to ½ the digitization frequency. All energy on the analogue tape at frequencies higher than the Nyquist frequency is 'aliased' to some frequency between 0 and ω_N in the data on the digital tape. (Blackman and Tukey, 1958). To minimize aliasing into the frequencies of interest a low pass filter is used to filter out energy above the Nyquist frequency prior to digitization. The filters used were a matched set which had a 3db. point at the Nyquist frequency and a 9db. per octave attenuation rate above that. Over the frequency range of interest the phase shifts introduced by the filters on each channel were all within 1° of one another. The cross spectral phases which depend only on the relative phase of one channel to another are thus only negligibly affected by the use of the filters. The attenuation of the spectral estimates below the Nyquist frequency is corrected for in SIMPLØT.

The upper frequency of analysis, the Nyquist frequency, is set by the choice of digitization frequency. At each separation the digitization frequency was picked so that the corresponding Nyquist wave number represented scale sizes about ¼ of the size of the separation. By this means only those turbulent scales of the same order of size as the separation were retained for analysis.

FTØR

FTØR is a computer program designed to evaluate (B.4) and (B.5) from the digitized data. It uses the Fast Fourier Transform to generate complex Fourier coefficients from every consecutive record, each of 1024 sample points from each channel of the digital tape. The number of records chosen for analysis was rather arbitrarily set at 40 for all of the runs. For each of the 40 records for each channel FTØR computes 512 complex coefficients.

SCØR

SCØR uses the complex coefficients outputted by FTØR and produces from these smoothed spectral, cospectral and quadspectral estimates. By combining the complex coefficients from one or two channels according to (B.6) it computes the desired cross spectra for all the wave numbers and for all the 40 records. It first averages the estimates over a quarter to a third octave bandwidths for each record. These averages are then themselves averaged over the 40 different records. The result of this procedure is a cross spectrum which is an estimate of the ensemble average from different realizations of the flow.

SCØR has an additional facility for computing cross spectra from the averages of the records. By this means it is possible to extend the analysis down to lower frequencies but because SCØR does little smoothing of these estimates any individual estimate must be considered fairly unreliable. In Figures 2 and 3 the estimates for the nine lowest wave numbers for each run are computed by this means.

RØTATE

The 3D sonic anemometer senses two horizontal components of velocity at 120° to one another. RØTATE transforms the spectra derived from these two components into the spectra of downwind velocity fluctuations and into the spectra of cross-stream fluctuations.

SIMPLØT

SIMPLØT is used primarily to correct the cross spectral estimates for the attenuation introduced by the A-D filter. Each of the SCØR spectral estimates is simply multiplied by the inverse of the attenuation factor of the filter at that frequency.

In SIMPLØT too the hot wire anemometers are calibrated. The output of RØTATE gives the integrals under the spectra of the downwind velocity fluctuations measured by the sonic as well as the integrals under the spectra of the uncalibrated hot wire anemometers. The calibration used for a given hot wire was that necessary to make its integral over the lower wave numbers where the sonic is expected to give reliable results equal to the sonic integral over the same wave numbers. Because the sonic anemometer and the hot wire anemometers have slightly different shapes to their spectra due to their different operating characteristics and to their sensing the turbulence at different positions in space this calibration will be only roughly accurate. However, except for Figures 3 and 4 all of the hot wire cross spectra are plotted in a normalized form which eliminates the need for any hot wire calibration at all.

Leakage Correction

All of the observed cross spectra are corrected using (B.11) for the leakage of energy from one wave number to another resulting from the analysis of finite data records. Because the majority of the energy in typical spectra and cospectra occurred in the lower wave numbers of analysis the correction term for them was approximated from their low wave number estimates using (B.9). The magnitude of the correction term which was about the same for both spectra and cospectra ranged between 15% of the spectral level at $k_1\delta = 1.0$ for the 2 cm. separation down to 1% at $k_1\delta = 1.0$ for the 1.8 m. separation. The magnitudes of the corrections to the quadspectra, which had little energy at low wave numbers, were very small.

PLØTTING

Two different methods were used for plotting the results. The hot wire spectra shown in Figures 3 and 4 and the sonic spectra shown in Figure 2 are plots of the form $\log_{10}\left(k_1\Phi_u(k\ )\right)$ versus $\log_{10}(k_1 z)$ where z is 2 m. $k_1\Phi_u(k_1)$ is the energy in a wave number band of width $\frac{dk_1}{k_1}$ whereas $k_1 z$ is a non dimensional wave number. The theoretical and the observed cospectra plotted in Figures 6, 7, and 8 are all normalized by the appropriate spectrum. The abscissa axis in each case is $\log_{10}(k_1\delta)$. The cospectra from the different separations should be approximately similar with respect to $k_1\delta$.